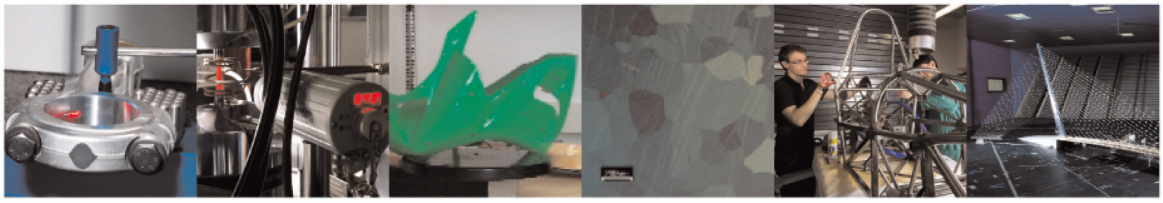

A vibration-based approach for health monitoring of tie-rods under uncertain environmental conditions

F. Lucà, S. Manzoni, A. Cigada, L. Frate

This is a post-peer-review, pre-copyedit version of an article published in *Mechanical Systems and Signal Processing*. The final authenticated version is available online at:
http://dx.doi.org/10.1016/j.ymssp.2021.108547

DIPARTIMENTO DI MECCANICA ■ POLITECNICO DI MILANO
via G. La Masa, 1 ■ 20156 Milano ■ EMAIL (PEC): pecmecc@cert.polimi.it
http://www.mecc.polimi.it
Rev. 0

A vibration-based approach for health monitoring of tie-rods under uncertain environmental conditions

F. Lucà[1], S. Manzoni[1], A. Cigada[1], L. Frate[1]

1. Politecnico di Milano – Department of Mechanical Engineering, Via La Masa, 34 – 20156 Milan (Italy)

Corresponding author: F. Lucà (francescantonio.luca@polimi.it)

ABSTRACT

This work proposes a vibration-based damage detection approach for axially loaded beam-type structures. The potential of the adopted approach is shown with an application to structural health monitoring of tie-rods: these elements, widely used in civil structures to balance horizontal forces in arches, are normally subject to a significant change of the axial load under environmental and operating conditions. The related changes in the modal parameters are usually greater than those caused by damage, at least at an early stage, making it hard to separate the different effects. In this work, the confounding effect of environmental factors is filtered out by considering more than one vibration mode at a time, thus framing damage detection as a multivariate outlier detection problem. Two damage indexes are presented, based on modal parameters (eigenfrequencies and mode shapes) and a multivariate metric (the Mahalanobis squared distance). The reasons behind the potential of the proposed framework are shown on simulated data first. Then, this strategy is validated on data coming from experimental tests, where two nominally identical tie-rods have been monitored for several months under the effects of realistic environmental and operational conditions. Both indexes proved to be weakly influenced by environmental variations, mainly related to temperature, and thus proved to be suitable for automatic damage detection.

Keywords: damage detection, tie-rod, structural health monitoring, operational modal analysis, continuous monitoring, statistical pattern recognition

1. Introduction

In recent years, structural health monitoring systems are increasingly adopted to assess whether an operating structure is still able to meet the required performances and safety standards, despite aging and degradation [1]. The development of automatic damage detection strategies plays a fundamental role in the transition from time-based inspections to condition-based monitoring, allowing for a more effective maintenance of mechanical, civil and aerospace structures. This result can be achieved if the information contained in the data acquired by sensors placed on the monitored structures is extracted through synthetic indicators that can point out the presence of damage at an early stage [2].

Many attempts to define effective damage features can be found in the literature, mainly based on vibration data, since structural changes caused by damage manifest themselves as changes in the dynamic response features [3,4]. However, the effect of environmental and operational variations, particularly temperature [5], represents one of the main obstacles in translating structural health monitoring strategies from research to operating structures. Many studies highlighted that temperature variations may cause changes in structural vibration properties which can be greater than those caused by damage [6]. Although

different techniques have been proposed to overcome this limit, no general and effective methods have been developed.

In this paper, a damage detection approach is proposed to separate the effect of damage by those caused by environmental variations in beam-type structures, widely used in the field of engineering structures (e.g. diagonal braces of a truss girder, struts and ties of a space truss structure, tie-rods of arches and vaults). Into details, beams subjected to axial-load are considered, i.e. tensioned beams. These structures are subject to change of the axial load during their life, mainly related to environmental effects and loading conditions. This reflects into changes of the dynamic response, making vibration-based damage detection in tensioned beams a hard task.

In this work, damage detection in tie-rods has been selected as case study. Tie-rods are metallic elements widely used in historical and modern civil structures to balance the lateral force at the base of arches and vaults, working under axial loads (however, the proposed damage detection strategy can be adopted on any beam-like structure subject to axial load). Tie-rods are fundamental in order to grant the overall structural equilibrium since a failure of these elements may result in a global structure failure. An interesting aspect of operating tie-rods is that, in real cases, there is a considerable uncertainty about the knowledge of the axial load to which they are subjected. Indeed, from a review of the state of the art on tie-rods, attention from researchers has been mainly paid to the identification of the tensile force. This is done with the aim of identifying changes in the axial loads transmitted by the arch base, to obtain information about the overall structural behaviour [7] rather than assessing the damage of tie-rods. Since the only possible way to have an accurate measurement of the axial load is the application of strain gauges or load cells prior to tie-rod tensioning, which is obviously impossible in case of existing buildings, many techniques have been developed based on static [8,9], static-dynamic [10] or fully dynamic [11] in situ indirect measurements. Concerning dynamic techniques, they generally rely on vibration measurements, even if recently acoustic-based measurements have been adopted too [12]. The axial load is estimated by solving a challenging nonlinear and potentially ill-conditioned inverse problem, since modal parameters are not only representative of the axial force, but also of other physical variables and boundary conditions. Different approaches have been proposed to identify the unknown parameters analytically [13,14] or through minimization between the experimental and the theoretical modal parameters [15,16], set inversion [17], model updating [18] and genetic algorithms [19].

Although many methods for the axial-load estimation may be found in literature, minor attention has been paid to the existence of possible damage in tie-rods, since all the developed models, both analytical and based on finite element models, do not take into account the presence of damage. On the contrary, being able to assess whether damage is present in the tie-rod is important for structural health monitoring purposes. Indeed, deteriorative phenomena such as the chemical corrosion can cause a decrease in the tie-rod strength, affecting its performances.

Damage identification for these elements cannot be carried out by monitoring the tensile force because multiple disturbing sources cause variations in the axial load that cannot be related to actual variations of the health state of the tie-rod, e.g. temperature variations cause changes in the material characteristics of both the tie-rod and of the structure, in turn reflecting into variations of the axial load.

Recently, a technique for the identification of cracks in tie-rods has been presented in [20]. Combining the information coming from the analysis of the rod dynamic behaviour and the estimation of the flexural compliance, the method has proven to be effective in detecting the presence of cracks in laboratory tests. Even if the results confirmed that a cracked tie-rod behaves differently from a healthy one, the approach seems to fit well in situations where a significant change in the dynamic response can be directly measured in terms of eigenfrequency variations. Thus, in real situations, where the confounding influence of the axial

load can add a source of variability, the approach cannot be directly adopted unless a reference healthy beam is available, to separate out the contribution of the axial load.

In this context, this work overcomes these limitations by proposing an easy-to apply vibration-based damage detection algorithm which allows for a separation between the environmental and the damage effect. The approach is based on the identification of few simple modal parameters: eigenfrequencies and mode shapes. The main difference with respect to [20] is that damage is not detected in terms of variation of modal parameters, rather following a statistical pattern recognition approach that allows for the removal of the confounding effect caused by the axial load. Indeed, a crucial observation is that the presence of damage alters the relationship between the modal parameters of multiple vibration modes which can be considered as multiple variables of the same multivariate set. If a baseline set referring to the undamaged condition is available, damage detection becomes a multivariate outlier detection problem. Following these considerations, this work presents two damage indexes based on modal parameters and a multivariate metric: the Mahalanobis Squared Distance (MSD). The two indexes proved to be weakly influenced by the environmental and boundary conditions, resulting in being representative of the health state of a tie-rod. The main advantage with respect to the state of the art is that the effect of damage can be separated out from that of the axial load without the need for an estimate of the tie-rod tension and, moreover, without a reference structure. Another important aspect is that the extraction of the modal parameters required for the proposed framework can be done through the adoption of well-established operational modal analysis (OMA) techniques, as proved by different works presented in literature [21–23]. Since these techniques exploit the environmental excitation and only rely on the response measured with accelerometers placed on the monitored structures, no time-based inspections with specific in-situ experiments are required. Therefore, the proposed damage detection strategy can be applied in continuous, under operating conditions.

In the next section, the theoretical background is presented, together with the description of the proposed method. A brief recall of the vibration theory for a tensioned beam is presented first, in order to highlight the physical variables mostly contributing to the modal parameters of interest: eigenfrequencies and vibration modes. Some results coming from simulations on a finite element model (FEM) are then presented in Section 2.1 to discuss how the effects of damage may be distinguished from the effects of environmental variations by observing together parameters related to different vibration modes. Thus, an automatic damage detection strategy based on automatic OMA algorithms and multivariate statistics is presented in Section 2.2 and two damage indexes are proposed.

The test case used to assess the performances of the proposed approach is described in Section 3: a long-time monitoring system has been installed to measure vibrations on two nominally identical tie-rods located in the laboratory of Politecnico di Milano, in an environment where realistic variability of temperature and operating conditions can be observed. An FEM of the real specimen has been developed to simulate vibration data also accounting for environmental and operational variations (i.e., temperature variations and different excitation levels). The proposed strategy has been applied to detect the damage, which has been modelled as a local reduction of flexural stiffness; the simulation results are discussed in Section 4.

The experimental tests are described in Section 5. To test for the method sensitivity in a realistic environment, damage has been physically simulated on one of the two tie-rods through the addition of different masses chosen to cause variations of the proposed indexes similar to those caused by realistic damages. Damage has been simulated in two different positions: one close to the fixed ends and one at midspan.

In the end, conclusions are drawn in Section 6, along with further developments.

2. Transverse vibrations in tensioned beams and structural modification detection through tie-rod modal parameters

The theory of transverse vibrations in tensioned beams has been presented in many works in the literature, e.g. [24–26]. In this section, only the main points needed to explain the proposed damage detection strategy are reported, while the reader can refer to the above-mentioned works for an extended discussion. Into details, in order to understand how the modal parameters can be used to detect a structural modification in a tie-rod, it is useful to point out which physical variables mostly influence its dynamic behaviour.

Considering a beam of length L, with transverse section A, momentum of inertia of the section J, Young's modulus E and density ρ, the attention is here focused on the motion in the direction named z, orthogonal to the longitudinal axis of the beam, ξ (see Figure 1). The following assumptions are made:

- the material is homogeneous (E and ρ constant along the beam), isotropic and obeys Hooke's law;
- the beam is straight and of uniform cross-section (A and J constant along the beam);
- the beam is long compared to cross-sectional dimensions (the effects of shear deflection are neglected);
- only small transverse oscillations around the static equilibrium condition are considered.

The displacement along z is a function of the coordinate ξ and of the time t, thus it is indicated with the symbol $w(\xi, t)$.

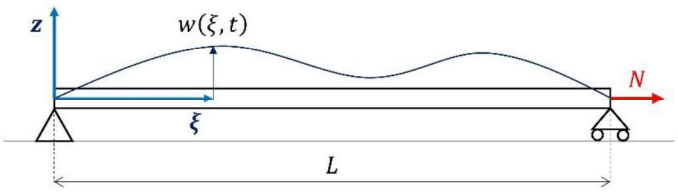

Figure 1: Tensioned beam

Under stationary conditions, the displacement along z has a specific shape $\Psi(\xi)$. The amplitudes in different points of the continuous system change, at different times, governed by a single time function $G(t)$**.** If the beam is subject to a constant axial load N, the stationary solution representing the free motion in transverse direction is described by the following equation [24]:

$$w(\xi,t) = \Psi(\xi)G(t) = \\ = [F_1\, sin(\gamma_1\xi) + F_2\, cos(\gamma_1\xi) + F_3\, sinh(\gamma_2\xi) + F_4\, cosh(\gamma_2\xi)][F_5\, sin(\omega t) + F_6\, cos(\omega t)] \quad (1)$$

where ω is the angular frequency. The constants F_1, F_2, F_3 and F_4 depend on the boundary conditions, F_5 and F_6 are the integration constants, to be defined by means of the initial conditions and γ_1 and γ_2 are defined as it follows [24]:

$$\gamma_1 = \sqrt{-\frac{N - \sqrt{N^2 + 4EJ\rho A\,\omega^2}}{2EJ}} \;\; ; \;\; \gamma_2 = \sqrt{\frac{N + \sqrt{N^2 + 4EJ\rho A\,\omega^2}}{2EJ}} \quad (2)$$

The boundary conditions must be imposed to obtain the expression of the system mode shapes $\phi_j(\xi) = [\Psi(\xi)]_{\omega=\omega_j}$, as well as the eigenfrequencies ω_j. From the equations above, the physical variables that influence the modal parameters of a homogeneous beam subject to an axial load are related to its geometry (A, J, L), material properties (E, ρ) and loading conditions (N). Furthermore, since the boundary conditions reflects on γ_1 and γ_2, the modal parameters of the tensioned beam are also influenced by the characteristics of the constraints.

Considering real tie-rods, if the geometrical parameters of the section can be measured, the length can sometimes be difficult to be estimated since the ends may be hidden by some structural elements. Material properties too are difficult to be estimated with enough accuracy, especially for ancient structures, unless some specific material tests are carried out. About the axial load, in most cases it is not possible to know its value through a direct in situ measurement.

In this paper, however, attention has been devoted to the development of a damage detection strategy able to highlight the occurrence of a structural modification in the tie-rod, with no need to know all the single physical variables influencing the dynamic behaviour of the tie rod. Thus, the proposed strategy will not rely on the identification of the axial load neither on the characteristics of the constraints. The idea is that eigenfrequencies and mode shapes might be used as synthetic indexes that can represent the current state of a monitored tie-rod, being representative of all the above-mentioned physical variables.

At this stage, one should point out that modal parameters of a tie-rod are highly sensitive to variability sources that are not related to a change in the state of health of the tie-rod. As an example, the thermal expansion of the material due to an increase in the environmental temperature may cause a decrease in the axial load of the tie rod and this will reflect in a decrease of the eigenfrequency values.

The crucial aspect of the proposed strategy relies on observing that the effect of damage on the modal parameters can be separated from those caused by variations in the axial load, if multiple vibration modes are considered together to define the state of health of the tie-rod, as explained in the next section.

2.1. Tie-rod modal parameters as features for damage detection

In this section, the core of the proposed strategy is explained, in order to point out the reasons why the proposed method can work in the real applications to detect damage on a tie-rod under operational conditions. To do so, the idea is to investigate if changes in the modal parameters caused by the environmental variations can be separated out from those caused by the occurrence of damage itself. To show such effects, simulated results coming from an FEM of a tie-rod with the same geometrical properties and characteristics of those composing the experimental test case, described later in Section 3.

The actual three-dimensional model of the experimental set-up (Figure 2a) has been used to develop an FEM with the commercial software Ansys. The geometry includes the tie-rod, which is divided into five contiguous sections named s1,s2,…,s5 (see Figure 2b), and the clamping system. Sections s2 and s4 are both characterized by a longitudinal length of 40 mm and they have been used to simulate damage, as explained in the following. Elements Hex20 (20 nodes hexahedral elements) have been employed to model the solid geometry. With reference to Figure 2a, the end side e1 is constrained in the directions ξ, y and z, while the end side e2 is constrained along y and z direction (rotations about ξ, y and z are not allowed for both ends), so that an axial load may be applied to the tie-rod. The size of the elements L_{elem} has been chosen such that a further refining of the mesh did not cause a significant change in the eigenfrequencies and mode shapes for the first ten bending vertical modes (the nominal data for the FEM are reported in Table 1, where E and ρ are respectively the nominal elastic modulus and density for aluminum).

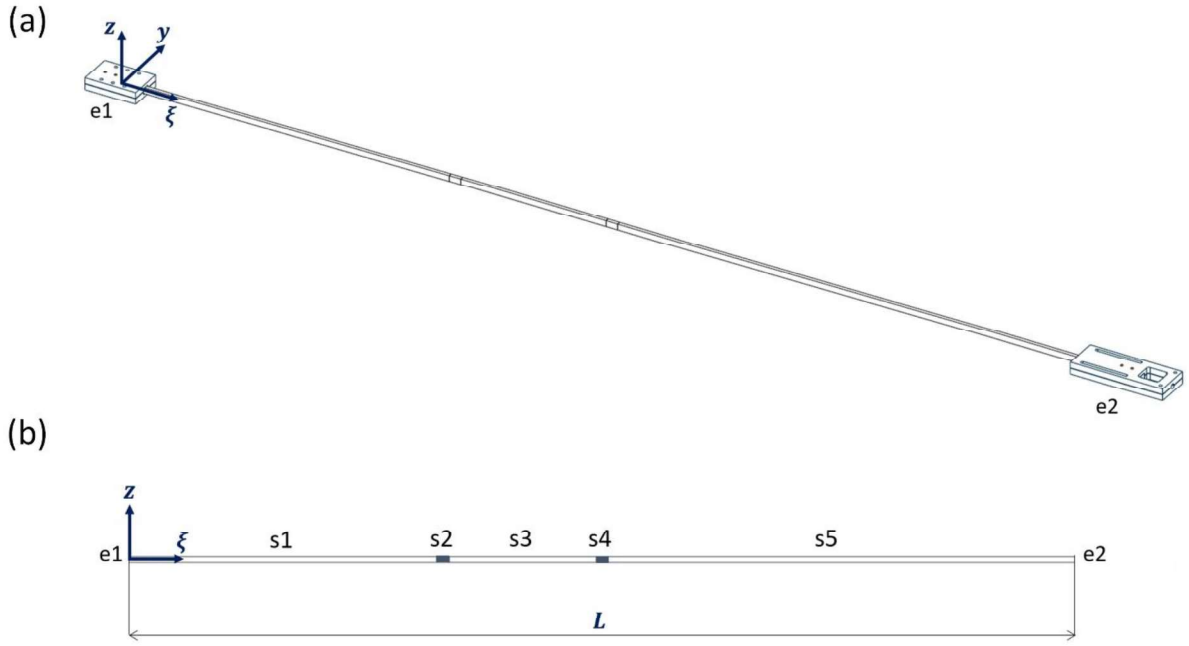

Figure 2: 3D geometry of the FEM which includes the tie-rod and the clamping system (a); detail of the sections that compose the beam (b)

E	ρ	L	L_{elem}	A
70 Gpa	$2700\ \text{kg/m}^3$	$4000\ \text{mm}$	7.5 mm	$15 \times 25\ \text{mm}^2$

Table 1: Nominal data for the FEM

No particular attention has been paid to simplify the model in order to increase the computational efficiency, since no FEM is required for the application of the proposed damage detection strategy. Indeed, in this work the FEM is only used to provide some examples that may be useful to better explain the reasons why the proposed strategy can be adopted to detect the damage in tie-rods. To do so, two different situations are now discussed: one where the axial load changes and the tie-rod is in a healthy state (i.e. the axial load changes because temperature changes while the tie-rod is not damaged), and one where a damage is considered for a given fixed value of the axial load (i.e. temperature is constant and the tie-rod is damaged).

Under reference conditions, all the tie-rod sections s1,s2,…,s5 have the same elastic modulus E^{ref} (the standard value for aluminum has been considered - the reasons behind this choice are discussed in Section 3); this value has been assumed equal to $70\ \text{GPa}$ and the axial load N^{ref} equal to 15 kN, which is a value consistent with what observed in real applications [27]. In the following, any deviation from the nominal condition will be quantified by the index $\Delta N = \left(1 - N/N^{\text{ref}}\right) \times 100$, where N indicates an axial load which is different from N^{ref}. Into details, the parameter ΔN is adopted to simulate variations of the axial load associated to temperature changes, when the tie-rod is in a healthy condition. By definition, as from the above formula, a positive value of ΔN indicates a decrease in the value of axial load.

Damage is then simulated in two different ways, by changing either the Young's Modulus or the local thickness of the tie-rod in only one of the two sections s2 and s4 at a time. In case a reduced value for the Young's modulus E is used for either section s2 or s4, a localized drop of the elastic modulus is quantified by $\Delta E = \left(1 - E/E^{\text{ref}}\right) \times 100$. It is worth noting that a decrease in the value of the elastic modulus is

represented by a positive ΔE. Similarly, a localized reduction of the thickness h of the tie-rod is quantified by $\Delta h = \left(1 - h/h^{\mathrm{ref}}\right) \times 100$, where $h^{\mathrm{ref}} = 25\ \mathrm{mm}$. Also in this case, a reduction of local thickness corresponds to a positive Δh.

In the following, eigenfrequencies and mode shapes are compared against a reference condition where no damage is present and the axial load is N^{ref}. The eigenfrequencies and mode shapes in the reference condition will be indicated with f_j^{ref} and $\underline{\phi}_j^{\mathrm{ref}}$ respectively, where $f_j = \omega_j/(2\pi)$. When a change in the simulation parameters is considered, its effect on the eigenfrequencies is quantified by the value $\Delta f_j = \left(1 - f_j/f_j^{\mathrm{ref}}\right) \times 100$, which indicates a variation of the j-th eigenfrequency in a new condition f_j with respect to the reference value f_j^{ref}. About mode shapes, the Modal Assurance Criterion (MAC) [28] is used to quantify the difference between the j-th mode shape in a new condition $\underline{\phi}_j$ and the reference $\underline{\phi}_j^{\mathrm{ref}}$:

$$MAC_j = MAC\left(\underline{\phi}_j, \underline{\phi}_j^{\mathrm{ref}}\right) = \frac{\left|\underline{\phi}_j^{\mathrm{ref}^T}\, \underline{\phi}_j\right|^2}{\left(\underline{\phi}_j^{\mathrm{ref}^T}\, \underline{\phi}_j^{\mathrm{ref}}\right)\left(\underline{\phi}_j{}^T\, \underline{\phi}_j\right)} \tag{3}$$

where $\underline{\phi}_j$ and $\underline{\phi}_j^{\mathrm{ref}}$ are column vectors containing the mode shape components at the nodes of the FEM that are used to reconstruct the j-th mode shape and the suffix "T" indicates the transpose. The MAC is bounded between 0 and 1, with 1 indicating equal mode shapes (i.e., the mode shapes $\underline{\phi}_j$ and $\underline{\phi}_j^{\mathrm{ref}}$ represent the same motion only scaled by a constant) while a value near 0 shows that the modes are not equal.

For simulations, four nodes have been selected corresponding to the same positions of the four accelerometers used in the tests, at $\xi = \frac{L}{20}, \frac{L}{10}, \frac{L}{3}, \frac{L}{2}$ (L is the beam length). The results will be presented for the first ten bending vertical modes, where the first five odd modes (Mode 1, Mode 3, …, Mode 9) are the first five symmetric modes and the first five even modes (Mode 2, Mode 4, …, Mode 10) are the first five antisymmetric modes of the tie-rod.

As a first step, only a reduction in the axial load is considered with ΔN ranging between 0% and 60%, without simulating damage (i.e. $\Delta E = 0\%$ and $\Delta h = 0\%$ for both sections s2 and s4). Figure 3a shows the effect of the change in the axial load on the first ten eigenfrequencies. The variations on the axial load mainly affect the lower eigenfrequencies and the effect is progressively less evident on the higher eigenfrequencies. Thus, for any given ΔN, it is always possible to state that $\Delta f_j > \Delta f_{j+1}$.

By observing the trend of the MAC shown in Figure 3b, it is noted that the effect of the axial load variation is almost negligible on the mode shapes, since MAC values are very close to 1 even when ΔN is 60 %.

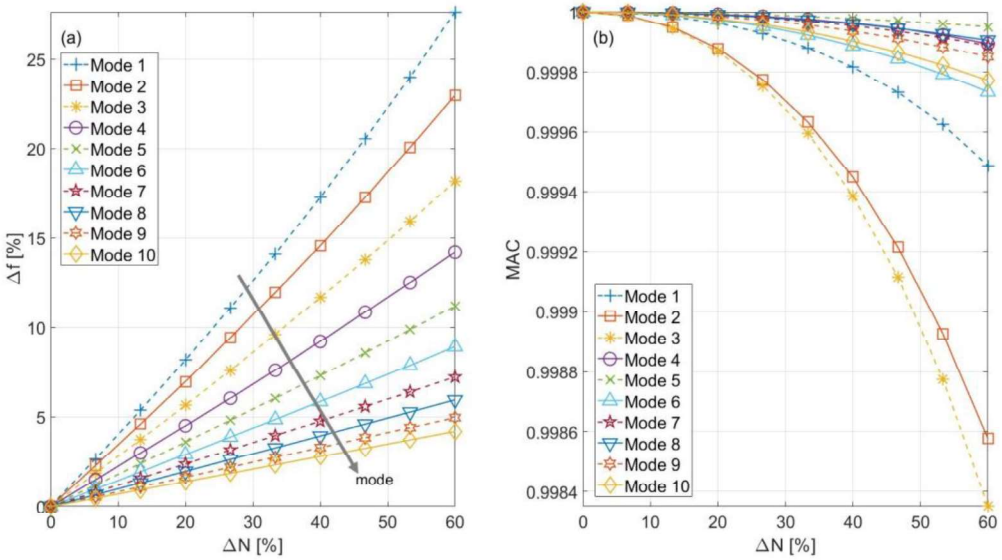

Figure 3: Effect of a reduction of the axial load on the first ten eigenfrequencies (a) and MAC (b)

Introducing damage in the tie-rod, for a given value of axial load, it is possible to observe a different effect on the modal parameters. The second set of simulations discussed here refers to a fixed value for the axial load ($\Delta N = 0\%$) and a ΔE which ranges from 0% to 50% for section s4 only, i.e. a damage at mid-span; results are shown in Figure 4. It is possible to note that the presence the described damage causes significantly smaller values of both Δf and MAC with respect to those caused by the variation of the axial load (compare Figure 4 and Figure 3). As an example, the eigenfrequency that shows the highest values for Δf, in presence of damage in s4, is considered: in this case, mode number 9 shows the highest values for Δf in Figure 4a, with a Δf equal to 0.88% when ΔE is equal to 50%. As it is possible to observe by comparing this value with those observed in Figure 3a, a similar Δf can be obtained in case of a small reduction of the axial load (around 11%). Thus, even if a change in the value of the most sensitive eigenfrequency is considered as a damage feature, the confounding effect of temperature would not allow for a damage detection. Detecting damage through a change in the MAC values (see Figure 4b) seems to be even tougher, with MAC values very close in magnitude to those observed in Figure 3b. Considering that in real applications the axial load is strongly influenced by environmental effects, it seems clear that observing the effect of damage on modal parameters, referring to individual vibration modes, would lead to a difficult task if the aim is damage detection.

However, a second remark is crucial for the proposed strategy: due to the presence of a local damage, the pattern of both eigenfrequencies and MAC changes in a peculiar way. In the case where damage is in the center of the tie-rod, representing a modal node for even vibration modes, only modal parameters associated to the odd modes are affected, as indicated by dashed lines with different markers in Figure 4a and Figure 4b. In this case, as opposed to what happens when the axial load changes, the higher the mode considered, the higher the effect is and the relationship $\Delta f_j > \Delta f_{j+1}$, previously observed in Figure 3a, does not hold anymore. A clear pattern can be noted in Figure 4b, where the MAC of odd modes is lower than the MAC associated to even modes, with higher modes that are more sensitive than lower modes, when damage is simulated at midspan. Therefore, the presence of damage alters the order of the curves with respect to what occurs when only the axial load changes.

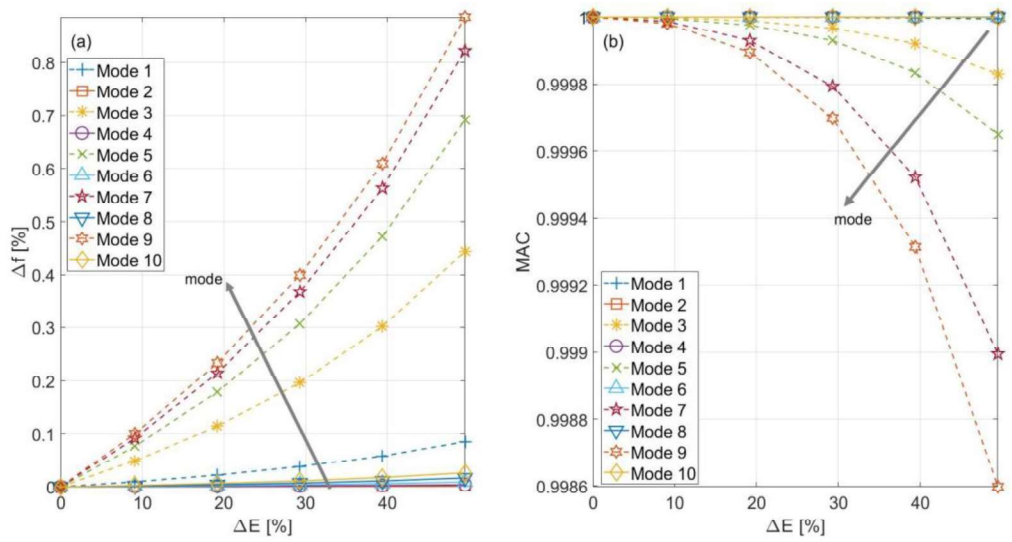

Figure 4: Effect of a reduction of the elastic modulus of section s4 on the first ten eigenfrequencies (a) and MAC (b)

The same remarks can be made by observing the results obtained by simulating damage as a reduction of local thickness at midspan, reported in Figure 5. Also in this case, the main difference between the effect of the axial load and the effect of damage is not related to the magnitude of Δf and MAC (compare Figure 5 and Figure 3) but to their pattern, with curves associated to odd vibration modes that change due to the local reduction of thickness. Furthermore, since the first eigenfrequency changes in the opposite direction with respect to the higher odd modes, the effect of the local reduction of thickness has a more evident effect on the pattern of Δf curves if compared to a local reduction of Young's modulus (compare Figure 5a and Figure 4a). No significative differences can be noted by comparing MAC trends of Figure 5b and Figure 4b.

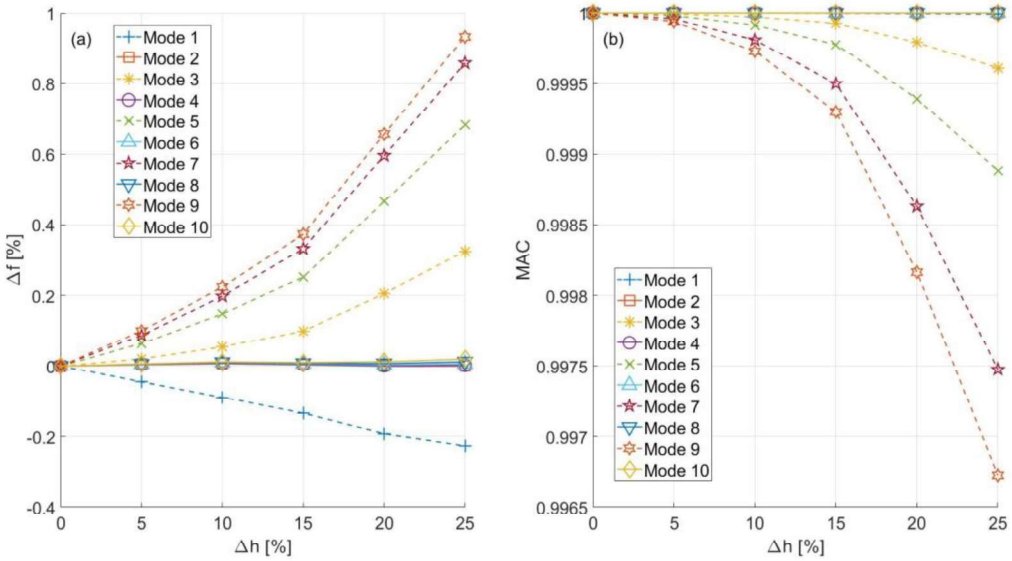

Figure 5: Effect of a reduction of thickness of section s4 on the first ten eigenfrequencies (a) and MAC (b)

Another example is reported in Figure 6, where a decrease of Young's Modulus is applied to section s2 only (again, $\Delta N = 0\%$). In this case damage is simulated in a position that is not a node for the first ten eigenfrequencies, thus representing a more general case. Also in this case, by observing Figure 6, it is possible to see that the effect of damage in terms of Δf and MAC is less evident than that caused by the axial load. This can be stated by comparing the values in Figure 6a and Figure 6b with those reported in Figure 3a and Figure 3b, respectively. Nevertheless, in this case too, the order of the curves changes in a clear way and this can point out the presence of damage in the tie-rod. Indeed, the relationship $\Delta f_j > \Delta f_{j+1}$ previously seen in Figure 3a does not hold anymore, with modes 8 and 5 that are respectively the first and second most sensitive modes, as from Figure 6a. Also, the order of the MAC curves in Figure 6b is different from that observed in Figure 3b and a direct comparison points out that a change occurred with respect to the condition when the tie-rod was undamaged. In addition, the patterns reported in Figure 6 are different from those reported in Figure 4, where only odd modes were sensitive to damage: this is also important because it is possible to distinguish different effects when damage is present in different sections of the tie-rod.

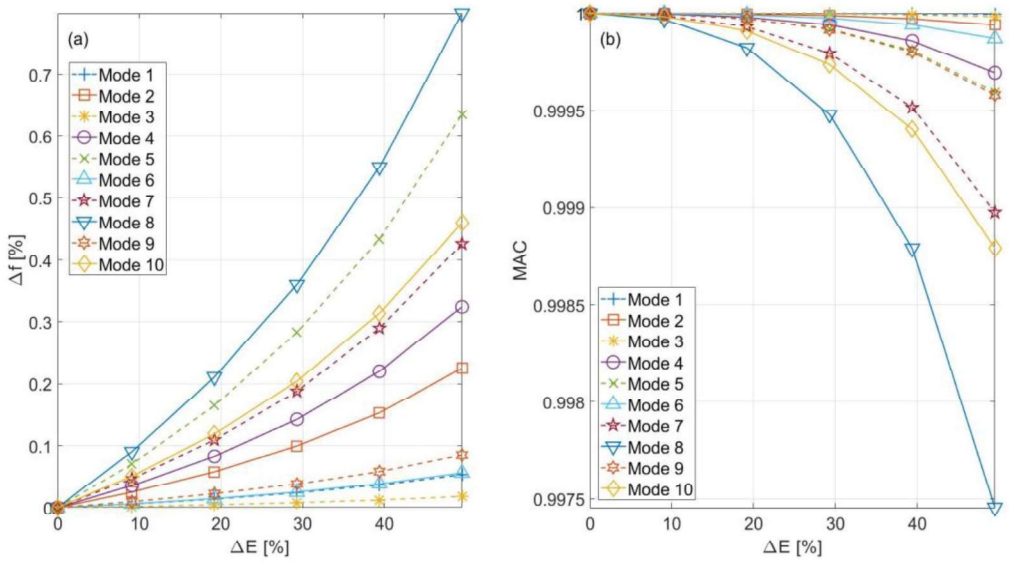

Figure 6: Effect of a reduction of the elastic modulus of section s2 on the first ten eigenfrequencies (a) and MAC (b)

The same observations apply to the case of a local reduction of thickness in section s2 (Figure 7). Also in this case, the order of Δf and MAC curves is different from both that caused by a change of axial load (compare Figure 7 and Figure 3) and that caused by damage at midspan (compare Figure 7 and Figure 5).

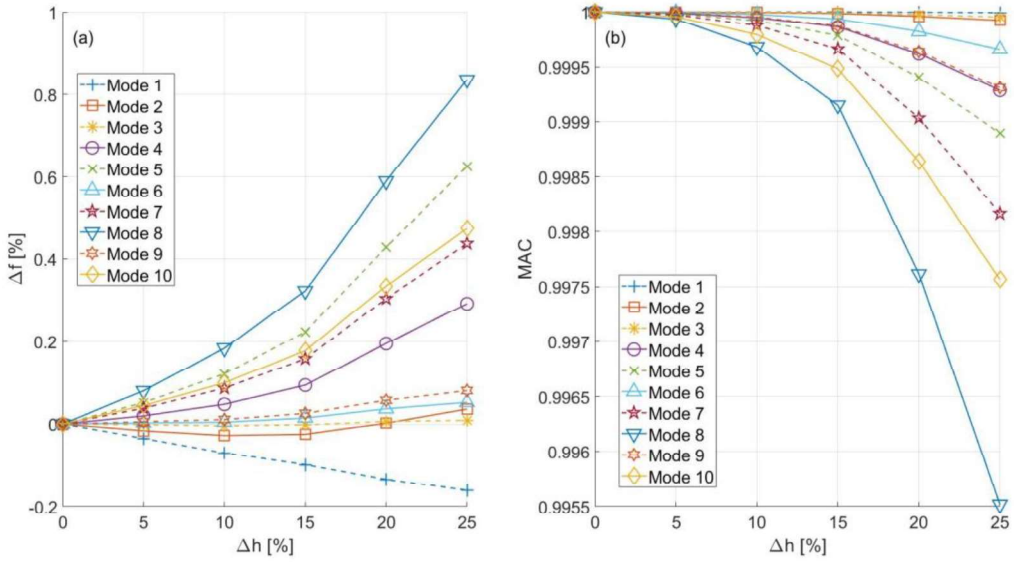

Figure 7: Effect of a reduction of thickness of section s2 on the first ten eigenfrequencies (a) and MAC (b)

Therefore, the main outcome of this preliminary analysis is that the effect of the damage can be distinguished from the effect of a change in the axial load (and, thus, also of the temperature) by considering together modal parameters of different vibration modes. Therefore, an effective damage detection strategy must detect changes in the pattern of modal parameters of multiple vibration modes, considered together, rather than variations in the modal parameters of single vibration modes.

Starting from this evidence, a strategy has been developed to detect damage in tie-rods under real environmental and operational changes. The next section describes into details how a well-known OMA technique, combined with tools related to multivariate analysis, may be used to define an effective strategy for real applications.

2.2. Monitoring strategy

The procedure of extracting the modal parameters and use them as indicators of the health state of a tie-rod is presented in this section. As it will be shown in the following, the proposed vibration-based strategy may allow for a continuous monitoring of the health state of the tie-rod under its operational conditions, without carrying out specific timed inspections. Indeed, the eigenfrequencies and mode shapes can be identified from the dynamic structural response through the adoption of OMA. Furthermore, the procedure can be successfully automated as shown by some recent papers about fully automated OMA [29–33]. In this work, the polyreference least-square complex frequency-domain method (PLSCFD) [34] has been used to identify the eigenfrequencies and mode shapes. Nevertheless, the concepts behind the proposed strategy may also be extended to other cases where other modal identification algorithms [35] can be adopted to extract the required modal parameters.

Considering a real case, a number of S accelerometers are used to measure the response of the monitored tie-rod to environmental excitation, for a finite amount of time T. Adopting a given value of sampling frequency f_{samp}, only a number of vibration modes M can be identified in the frequency range between 0 Hz and $f_{\mathrm{samp}}/2$, by applying the PLSCFD algorithm. For each j-th mode, with $j = 1, \dots, M$, it is possible to identify the eigenfrequency f_j and the related mode shape vector $\underline{\phi}_j$:

$$\underline{\phi}_j = \{\phi_{j,1}, \phi_{j,2}, \dots, \phi_{j,s}, \dots, \phi_{j,S}\}^T \tag{4}$$

where $\phi_{j,s}$ is the modal coordinate for the j-th vibration mode in the s-th degree of freedom (thus estimated by the s-th sensor), with $s = 1, \dots, S$. If a reference vector $\underline{\phi}_j^{\text{ref}}$ is the j-th vibration mode shape evaluated under reference conditions, the scalar coefficient $MAC_j = MAC\left(\underline{\phi}_j, \underline{\phi}_j^{\text{ref}}\right)$ can be used to quantify whether there is a correspondence between $\underline{\phi}_j$ and $\underline{\phi}_j^{\text{ref}}$.

Considering all the M identified vibration modes, results may be arranged in two vectors $\underline{f}$ and $\underline{MAC}$, defined as it follows:

$$\underline{f} = \{f_1, f_2, \dots, f_j, \dots, f_M\}^T \quad and \quad \underline{MAC} = \{MAC_1, MAC_2, \dots, MAC_j, \dots, MAC_M\}^T \tag{5}$$

If instead of considering only one record of duration T a set of N_{rec} records is considered, all characterized by a duration T, the PLSCFD method can be applied N_{rec} times. For every i-th record, with $i = 1, \dots, N_{\text{rec}}$, two vectors $\underline{f_i}$ and $\underline{MAC_i}$ may be evaluated. Into details, every j-th element of $\underline{MAC_i}$ is calculated with respect to the same fixed $\underline{\phi}_j^{\text{ref}}$, according to Eq. (3). The results may be arranged in two matrixes defined as it follows:

$$[f] = \begin{Bmatrix} \underline{f_1}^T \\ \underline{f_2}^T \\ \vdots \\ \underline{f_i}^T \\ \vdots \\ \underline{f_{N_{\text{rec}}}}^T \end{Bmatrix} \quad and \quad [MAC] = \begin{Bmatrix} \underline{MAC_1}^T \\ \underline{MAC_2}^T \\ \vdots \\ \underline{MAC_i}^T \\ \vdots \\ \underline{MAC}_{N_{\text{rec}}}^T \end{Bmatrix} \tag{6}$$

both with N_{rec} rows and M columns. Matrixes $[f]$ and $[MAC]$ are multivariate feature set, where each row represents an observation of the M variables.

When a new record of vibration data of duration T is available, the eigenfrequencies and MAC coefficients can be calculated and arranged in the vectors $\underline{f}^{\text{new}}$ and $\underline{MAC}^{\text{new}}$. Each of these two vectors represents a new observation of the multivariate feature sets $[f]$ and $[MAC]$ respectively and the Mahalanobis squared distance (MSD) [36,37], which is a common metric used in multivariate statistics, can be used for outlier detection.

Considering a generic matrix $[f]_{(N_{\text{rec}} \times M)}$ with N_{rec} rows and M columns (the same discussion is valid for a generic matrix $[MAC]_{(N_{\text{rec}} \times M)}$), characterized by multivariate mean vector $\underline{\mu_f}_{(M \times 1)}$ and covariance matrix $\left[\Sigma_f\right]_{(M \times M)}$, the MSD between the vector $\underline{f}^{\text{new}}{}_{(M \times 1)}$ and $[f]$ is defined according to:

$$MSD\left(\underline{f}^{\text{new}}, [f]\right) = \left(\underline{f}^{\text{new}} - \underline{\mu_f}\right)^T \left[\Sigma_f\right]^{-1} \left(\underline{f}^{\text{new}} - \underline{\mu_f}\right) \tag{7}$$

where the suffix "-1" means the inverse. The multivariate mean vector $\underline{\mu_f}$ and covariance matrix $\left[\Sigma_f\right]$ are reported in extended form in APPENDIX A.

The MSD, which is a scalar, can be used to state whether the vector $\underline{f}^{\text{new}}$ can be considered an outlier with respect to the multivariate set $[f]$. For the proposed approach, a number of records of vibration data

$N_{\mathrm{rec}}^{\mathrm{base}}$ must be acquired when the structure is in a reference condition, i.e. when the structure is in a healthy state. If $[f]$ and $[MAC]$ are calculated on a training set, they represent the baseline for the outlier detection and can be referred to as $[f]^{\mathrm{base}}$ and $[MAC]^{\mathrm{base}}$. According to Eq. (7), two damage indexes can be defined as it follows:

$$DI_1 = MSD\left(\underline{f}^{\mathrm{new}}, [f]^{\mathrm{base}}\right) \tag{8}$$

and

$$DI_2 = MSD\left(\underline{MAC}^{\mathrm{new}}, [MAC]^{\mathrm{base}}\right) \tag{9}$$

where multivariate mean vectors and covariance matrixes are evaluated on the baseline set.

These two damage indexes can be checked against a threshold t_{exc} that can be calculated following the procedure explained in [36] and reported in APPENDIX A. The value of t_{exc} only depends on the size of the baseline set and, thus, can be fixed once $N_{\mathrm{rec}}^{\mathrm{base}}$ and M are fixed. When the damage index defined on the eigenfrequencies is used, if $DI_1 > t_{\mathrm{exc}}$ the new observation is considered an outlier and damage is detected. The same is valid when the damage index is defined on the MAC coefficients and in that case the damage is assessed when $DI_2 > t_{\mathrm{exc}}$.

One of the major advantages of using the MSD is that this metric has proven to naturally filter out the variability in the training data, thus removing the environmental effects in damage detection while keeping a high sensitivity to structural changes [38]. In order to filter-out environmental effects, one should pay attention to using a proper baseline set containing the full range of environmental conditions, and to using a large enough feature vector in order to ensure some separability between the damage effects and the environmental effects [38].

In the following, the proposed strategy is tested on simulated data first, and then on real data coming from the long-time monitoring of two nominally identical tie-rods, in realistic operational and environmental conditions. A description of the test case is provided in the next section.

3. Test case

A test case has been selected to reproduce a realistic application of structural health monitoring of operating tie-rods. In this section, the structure designed and used for the experimental tests is described, together with the permanent monitoring system adopted.

The test case is composed by two nominally identical tie-rods made of aluminum, realized and then installed in the laboratories of Politecnico di Milano (Figure 8a).

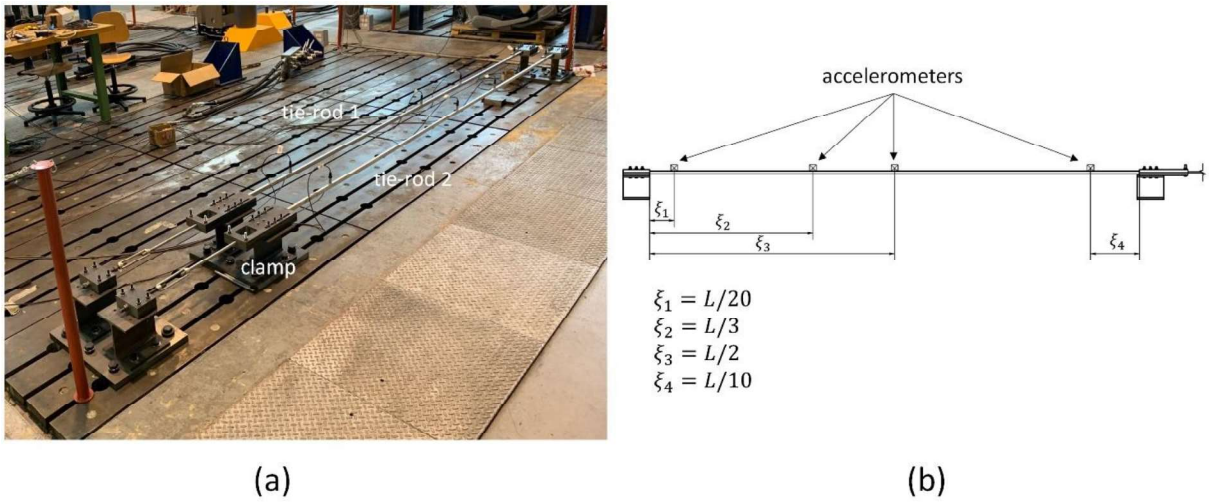

Figure 8: The experimental set-up (a) and the accelerometers layout (b)

The tie-rods are characterized by a cross-section $A = 15 \times 25\ \mathrm{mm}^2$ and free length $L = 4000\ \mathrm{mm}$. The material choice (i.e. aluminum) allowed for the use of relatively low values of axial load, still reproducing realistic conditions: indeed, considering that the average ratio between the operating axial stress and the yielding stress for standard applications is approximatively 22% [27], the axial load for an aluminum beam with cross-section A is approximately equal to 20 kN. Such force values simplified the design of the tensioning and clamping systems. With the proposed solution, a clamped-clamped configuration can be reproduced when the clamps are fixed through bolted joints.

During the tensioning procedure, which took place in October 2019, strain gauges composing a full Wheatstone bridge were installed on each of the two tie-rods and calibrated by using a load cell as reference. This procedure has allowed for a continuous monitoring of the axial load throughout the experimental tests. Even if this information is not required by the proposed damage detection strategy, it was collected to have a detailed description of the time-trend, because the axial load highly influences the dynamics of the tie-rod, as mentioned.

After the tensioning procedure, a preliminary experimental modal analysis has been carried out to characterize the dynamic properties of the two tie-rods and provide useful information to tune the FEM of the tie-rod. The eigenfrequencies for the first six vibration modes observed during the tests of October 2019 are reported in Table 2.

	Tie-rod 1	**Tie-rod 2**
f_1 [Hz]	13.89	14.17
f_2 [Hz]	30.98	31.64
f_3 [Hz]	53.36	54.46
f_4 [Hz]	81.82	83.24
f_5 [Hz]	116.55	118.66
f_6 [Hz]	157.95	160.40

Table 2: Modal parameters of the two tie-rods, identified during the preliminary phase (October 2019)

Moreover, the room temperature has been continuously measured by a calibrated thermocouple and stored together with the vibration data. This information has been used to characterize the daily variation of the axial load as a function of temperature. An example is reported in Figure 9, where the laboratory

temperature is compared with the axial load for the two tie-rods. This information has been used for the simulations described in Section 4.

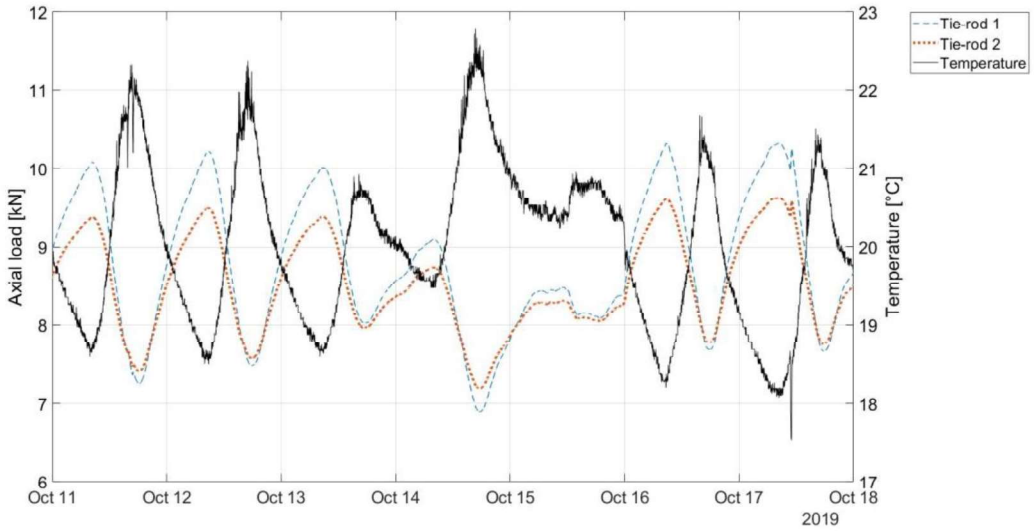

Figure 9: Axial load of the two tie-rods and temperature during one week between 11th October 2019 and 18th October 2019

The long-term monitoring of the two tie-rods started in December 2019, continuously measuring the response of the two tie-rods with eight accelerometers, four on each tie-rod, replicating a permanent structural health monitoring system. The adopted sensors are general purpose piezoelectric industrial accelerometers, PCB 603C01 (sensitivity 10.2 mV/(m/s^2), full-scale ±490 m/s^2). The acquisition system is composed by three NI 9234 modules with anti-aliasing filter on board. The sampling frequency has been set to 512 Hz and thus the first six eigenfrequencies are inside the allowed bandwidth: this is considered a good compromise between the need of continuous monitoring and the available space to store data (still a considerable amount of data has been stored with the above-mentioned acquisition parameters, approximately 3.62 Gb per day).

Once the number of observable vibration modes has been limited by the adopted sampling frequency, the choice for the number and positions of the sensors has been carried out trying to minimize the number of accelerometers, considering that in a real field application the use of few sensors is often desirable for both practical and economic reasons. The autoMAC matrix [28] has been evaluated for many different configurations, with layouts made by three to six accelerometers. The set-up showed in Figure 8b has been finally selected as the best compromise between using as few sensors as possible and obtaining a sufficient spatial resolution to describe and distinguish the first six bending mode shapes in vertical direction.

Nevertheless, the presence of many disturbances due to some testing machines in the surroundings of the test area did not allow for a stable automatic identification of the vibration modes above 100 Hz: but this too was part of the test plan, aimed at checking real operational conditions and not controlled laboratory ones. For the mentioned reasons, in the following, only the first four eigenfrequencies and vibration modes have been considered to calculate DI_1 and DI_2.

The results obtained by applying the proposed strategy to simulated data are presented in the following section.

4. Simulations

The FEM of a tie-rod (see Section 2.1) has been used to generate simulated vibration data, replicating the functioning of the monitoring system, according to the following procedure:

1. First, different frequency response functions (FRFs) have been evaluated between an input force applied close to one of the fixed ends of the tie-rod in the vertical direction and multiple output points, in terms of acceleration, for a given tie-rod axial load. More specifically, the longitudinal coordinates ξ of the output nodes have been chosen to be the same as the positions of the real sensors of the physical test, (see Figure 8b: $L/10$, $L/20$, $L/3$ and $L/2$). Thus, for a given axial load of the tie-rod, four FRFs have been estimated.
2. Step 1 has been repeated for different values of the axial load, chosen to replicate the effect of temperature on the tie-rod dynamic response.
3. The spectrum of the response has been obtained for each of the four measurement points by multiplying the spectrum of an input force by the FRFs evaluated in the previous steps. Once the spectrum of the response was available for a given measurement point and for a given temperature value, the corresponding time record has been reconstructed as a sum of harmonic components.
4. As a final step, a random signal has been added to the simulated data to reproduce the effect of electrical noise on the measurements.

For the simulations, a value of 600 N/°C has been considered to describe the dependence of the axial load from temperature, by observing the time-trends of temperature and axial load during the preliminary tests (see Figure 9). Five steps of 1 °C have been adopted to reproduce the daily changes observed in the laboratory. Thus, a variation of ±2 °C with respect to the average temperature has been considered as representative of the temperature fluctuations over a day. Discretizing the daily trends of temperature allowed for a reduced number of FEM simulations, while calculating the spectrum of the response in frequency domain and then reconstructing the vibration signals as a sum of its harmonic components resulted in a computationally efficient strategy.

To obtain data with a realistic signal-to-noise ratio, those measured on the real structure have been set as a reference. The signal-to-noise ratio of the real data has been estimated by assuming that the power of the electrical noise is the nominal value related to the accelerometers PCB 603C01 (spectral noise up to 10 Hz of $6.2 \times 10^3 \frac{\left(\frac{\mu m}{s^2}\right)^2}{Hz}$, assumed to be constant at any frequency, thus underestimating the accelerometer performances) multiplied by a factor of 2 to account for the additional noise introduced by the measurement chain. The signal-to-noise ratio of the real data has been estimated for different portions of the day, to reproduce operational variations. In fact, the excitation provided to the structure was maximum (thus the signal-to-noise ratio is maximum) during the mid-hours of working days (7 am to 6 pm). A medium level was observed during the evening, when traffic in the nearby of the laboratory is the only main excitation source (6 pm to midnight). The minimum signal-to-noise ratio was observed at night (0 am to 6 am), when both the activities in the laboratory and the traffic were almost absent. In addition, the signal-to-noise ratio did not reach maxima values at the weekends because the activities inside the laboratory were reduced. In order to account for this behaviour, three different signal-to-noise ratios have been considered when simulating data referring to a working day (33 dB, 53 dB and 59 dB), while only two levels (33 dB, 53 dB) have been used for a weekend day. In this way, the operational variability has been included in the simulated data.

A final dataset composed by 14 days of vibration data, with a sampling frequency of 400 Hz, has been used to test the damage indexes DI_1 and DI_2, as defined in Section 2.2. During the first seven days the structure has been simulated in the reference condition, i.e. no damage was present. At the beginning of the second

week, a local damage has been introduced, as a 25% decrease of the elastic modulus in section s2 ($\Delta E = 25\%$).

The automatic modal analysis has been carried out every ten minutes, calculating for every record the first four eigenfrequencies $f_1, f_2, \dots, f_4$ and the first four MAC values $MAC_1, MAC_2, \dots, MAC_4$. The results of the automatic identification are reported in Figure 10 and Figure 11.

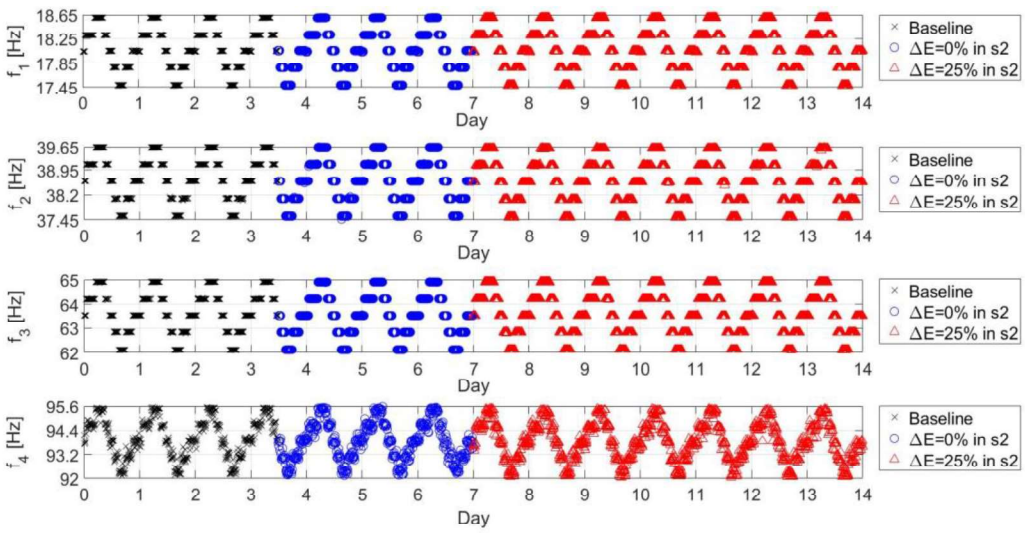

Figure 10: Identified eigenfrequencies for the tie-rod (simulated data). Black crosses indicate the observations used as baseline, blue circles are used to indicate undamaged data, red triangles refer to the damage condition

For the application of the damage detection strategy, the first half of the first week of data (black crosses in Figure 10, Figure 11) were set as baseline, representing the reference condition.

As it is possible to observe from Figure 10, the eigenfrequencies show a dispersion associated to the uncertainty of the modal identification and a daily trend that is associated to the daily trend of temperature. Indeed, no differences can be noticed in the final two days of the week, where the cyclical behaviour of the signal-to-noise ratio is different from the working days.

Looking at the time trends of the first four eigenfrequencies, it is not possible to detect any clear sign of the presence of damage, which should be clearly pointed out since the beginning of the second week (red triangles). Thus, it is possible to conclude that the spread of the identified frequencies and the environmental and operational changes make it difficult to develop an effective damage detection strategy based only on a single eigenfrequency value.

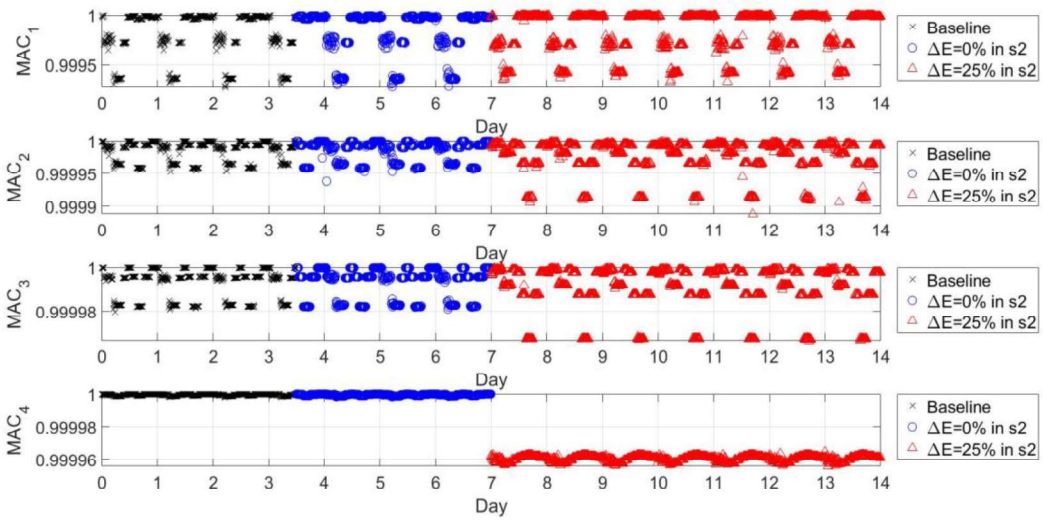

Figure 11: Identified MAC for the first four vibration modes of the tie-rod (simulated data). Black crosses indicate the observations used as baseline, blue circles are used to indicate undamaged data, red triangles refer to the damage condition

In Figure 11, the plot of the MAC for the first four vibration modes is reported. An important aspect is that, as already stated in Section 2.1, MAC values are very close to 1. Here, the effect of damage can be clearly detected by looking at the trend of MAC_4 which shows a discontinuity at the beginning of the second week of data acquisition, in agreement with what remarked in 2.1, i.e. the higher the vibration mode, the more sensitive the MAC is. Nevertheless, also in the case of MAC_4, the magnitude of the gap is very small and sometimes it may be masked by the spread associated to the identification error, when also uncertainty is accounted for.

Starting by the eigenfrequencies and MAC identified on simulated data and presented in Figure 10 and Figure 11, the damage indexes DI_1 and DI_2 have been calculated. The results are presented in Figure 12 and Figure 13, where the threshold t_{exc} already mentioned in Section 2.2 is evidenced by a black dashed horizontal line. In both figures, each marker indicates the MSD between the single observation of the modal parameter ($\underline{f}^{\mathrm{new}}$ or $\underline{MAC}^{\mathrm{new}}$) and the corresponding baseline matrix ($[f]^{\mathrm{base}}$ or $[MAC]^{\mathrm{base}}$).

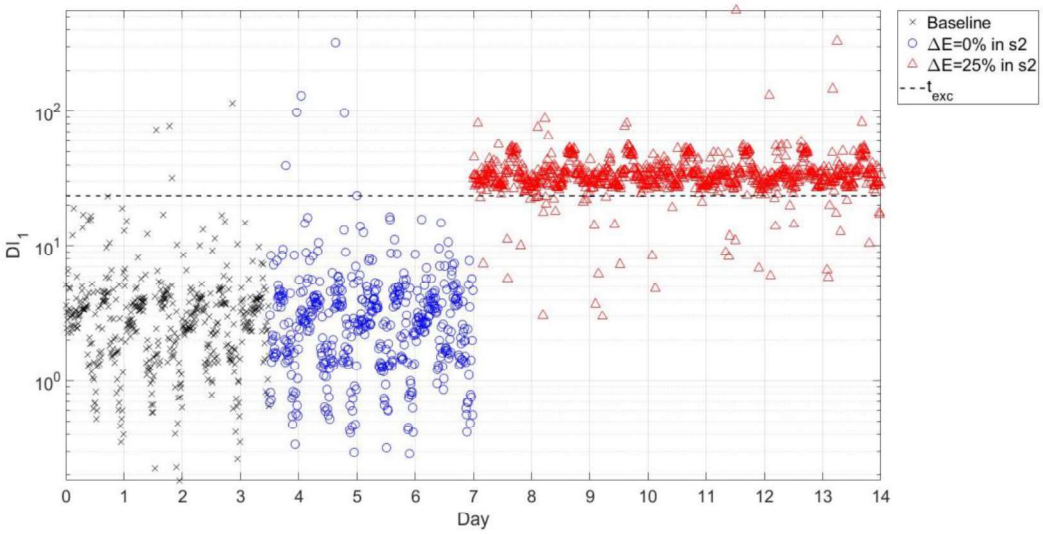

Figure 12: Damage index DI_1 for simulated data. Black crosses indicate the observations used as baseline, blue circles are used to indicate undamaged data, red triangles refer to the damage condition; the threshold t_{exc} is indicated by a black dashed line

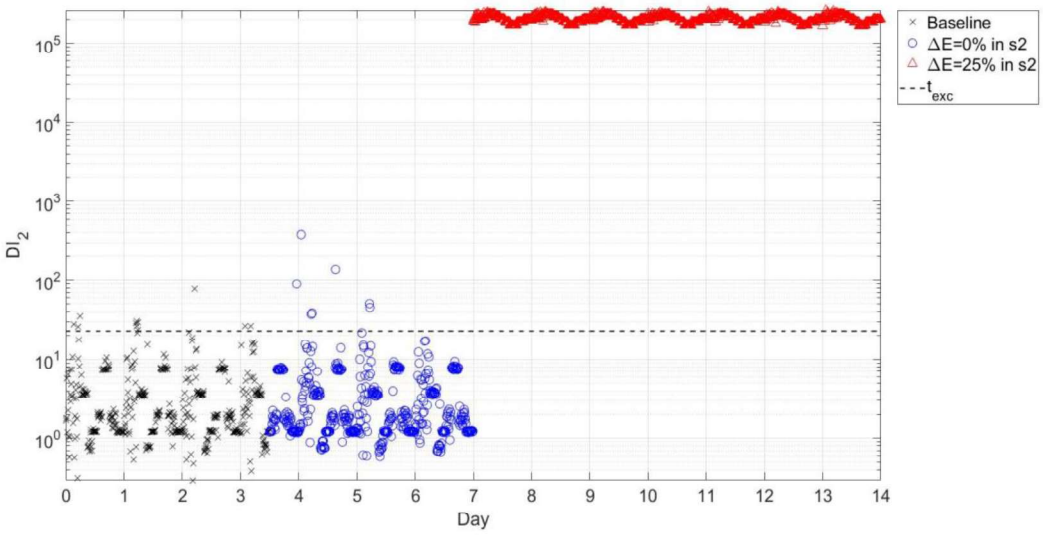

Figure 13: Damage index DI_2 for simulated data. Black crosses indicate the observations used as baseline, blue circles are used to indicate undamaged data, red triangles refer to the damage condition; the threshold t_{exc} is indicated by a black dashed line

As it is reasonable to expect, almost all the black crosses and blue circles should fall under the threshold, while red triangles should be above the threshold, pointing out that the new observations represent a different state of the monitored structure.

In Figure 12, it is possible to see that DI_1 is effective in highlighting the presence of damage, with the index above the threshold since the beginning of the second week. Thus, in this case the cyclical trend of the environmental and operational variations that was clear by observing the single eigenfrequencies (see Figure 10) is not creating any masking effect over the presence of damage. Furthermore, data referring to the undamaged scenario (blue circles) are in most part under the threshold, with similar values as those of the reference scenario. It is possible to see that few blue circles are above the threshold (false positives, i.e. the tie-rod is healthy but damage is detected) and few red triangles are below the threshold (false

negatives, i.e. the damage is present but it is not correctly detected). This behaviour is related to the error committed by the automatic OMA, which can be reduced by adjusting the OMA input parameters (e.g. number of averages for calculating the power- and cross-spectra, frequency resolution) [35,39,40]. This point will be further addressed at the end of Section 5, where results coming from a real case will be discussed and a stabilization criterion will be presented. By applying such a criterion, a decision on the state of health of the monitored tie-rod can be made such that it results weakly affected by the spread produced by the automatic modal identification error.

By looking at Figure 13, results are even more promising for index DI_2, where only few false positives and no false negatives are observed. Moreover, in this case, red triangles are way above the threshold. Conversely to what previously discussed for Figure 11 regarding MAC_4, DI_2 is around 10^5 when damage is present against values around 10^1 when the tie-rod is in healthy state, allowing for a clear separation between healthy and damaged structure.

The results coming from the simulations showed the potential of the proposed damage detection strategy: by considering only the first four vibration modes, both DI_1 and DI_2 proved to be more sensitive to structural modifications related to damage than to those caused by environmental and operational variations, thus being capable to detect damage in tie-rods. Into details, DI_2 seemed to be more sensitive than DI_1. The analysis has been extended to real data coming from the long-term monitoring of two real tie-rods to validate these conclusions. The results of the experimental tests are presented in the following section.

5. Experimental tests

The goal of the experimental tests was to verify the performances of the two damage detection indexes DI_1 and DI_2 when a real tie-rod is monitored under realistic operational and environmental conditions. To do so, two nominally identical tie-rods described in Section 3 have been monitored from 19th December 2019 to 15th March 2020.

At first, both tie-rods have been monitored under the same conditions, i.e. no structural modification was present, to build the baseline dataset for each of them. Then, a damage has been simulated on one of the two tie-rods, named tie-rod 1 from now on, with the addition of a concentrated mass. In this way, the dynamic properties of tie-rod 1 have been altered from the reference condition, with a simple strategy, often used in literature [41–45]. By adopting this strategy, different mass values and different positions have been used, without replacing the tie-rod. In addition to obvious economic advantages, this approach allowed avoiding the introduction of sources of variability only related to the tie-rod replacement procedure that could have magnified the difference between damage and the reference conditions.

Three different masses of 1%, 3% and 5% of the tie-rod total mass have been fixed in two positions, one very close to the clamp ($\xi = \mathrm{L}/10$) and one at midspan ($\xi = \mathrm{L}/2$); in the following, these two positions are referred to as “position 1” and “position 2” respectively. By preliminary simulations it has been observed that the addition of a 1% mass in s2 (see Section 4) causes changes in the modal parameters of the fourth vibration mode comparable to those caused by a 30% decrease of the elastic modulus ($\Delta E = 30\%$). The other two masses of 3% and 5% are set to represent more severe damage conditions, where the dynamic response of the tie-rod can be significantly changed (i.e. a failure in the constraints).

To validate the results, the other tie-rod (tie-rod 2) has always been kept in the reference conditions, i.e. no masses have been added. Indeed, if the considered damage index is above the threshold t_{exc} for tie-rod 1 when a mass is added, it is important to check that this does not occur for tie-rod 2 too, to double check that environmental or operational conditions do not cause any damage index changes.

The schedule of the tests is reported in Table 3, along with the labels adopted in the following to refer to a specific combination of mass value and position.

mass on rod 1 [%]	Position	Date	Label
0	-	19th Dec 2019 – 4th Jan 2020	T0
1	1	8th Jan 2020 – 15th Jan 2020	T1
3	1	15th Jan 2020 – 21st Jan 2020	T2
5	1	22nd Jan 2020 – 29th Jan 2020	T3
5	2	5th Feb 2020 – 12th Feb 2020	T4
3	2	27th Feb 2020 – 5th Mar 2020	T5
1	2	7th Mar 2020 – 14th Mar 2020	T6

Table 3: Scheduling of the experimental campaign

Through all the monitoring period, no control has been intentionally adopted on temperature (though measuring it) and environmental noise, so that the two tie-rods were observed in a very challenging and realistic scenario. The presence of working activities near the structures along with other testing machineries occasionally working, in addition to the generic presence of people in the laboratory created a high variability of operational loadings, not always just white noise, as required by operational modal analysis. This aspect sometimes caused a failure in the automatic modal identification procedure. However, sufficiently stable results were obtained by carrying out the identification every ten minutes.

When the presence of extraordinary events such as high energy impulses caused by human activities close to the experimental set-up did not allow for the identification of even one of the four considered vibration modes, results were discarded without losing generality, thanks to the very high data redundancy. By keeping the duration of each analysis equal to ten minutes, a negligible quantity of data has been discarded.

In Figure 14, the identified eigenfrequencies are reported for the two tie-rods in the considered period. Vertical lines are used to indicate different structural conditions according to Table 3. The gaps are associated to periods where the system was not acquiring data, while the experimental set-up was not modified.

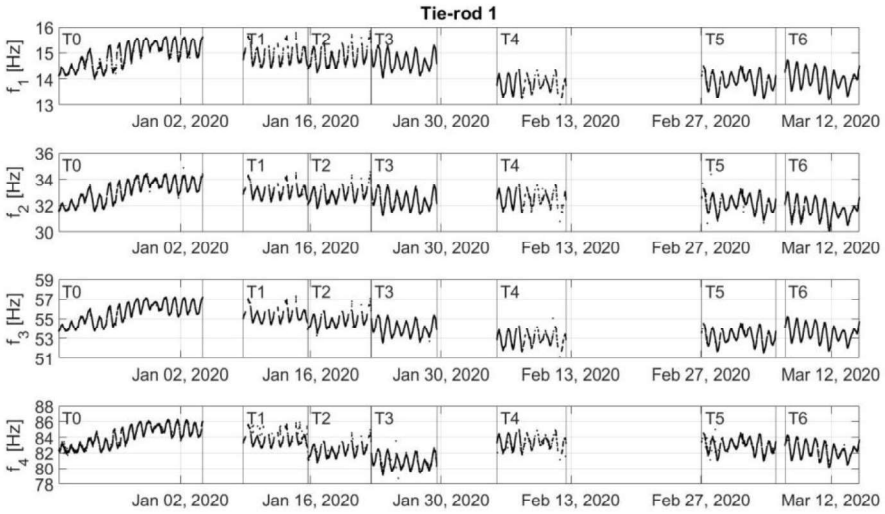

Figure 14: First four eigenfrequencies identified during the experimental campaign for tie-rod 1

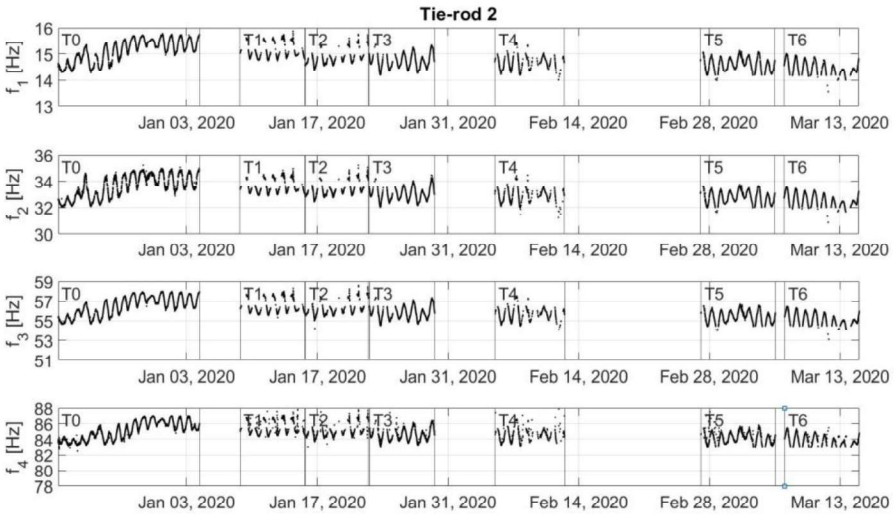

Figure 15: First four eigenfrequencies identified during the experimental campaign for tie-rod 2

As it is possible to see, the time trends are characterized by strong variability, and eigenfrequencies show both daily and long-term trends. As expected, due to the daily and seasonal trends of temperature, the axial load of the tie-rods continuously changes, causing changes in the modal parameters too, hiding the structural variation. Indeed, by simply looking at the trends in time for the eigenfrequencies of tie-rod 1 in Figure 14, it is not possible to clearly assess whether the concentrated masses were applied on the structure or not. In fact, by comparing any single configuration against the reference, both tie-rod 1 and tie-rod 2 (Figure 15) show similar behaviours.

If the trends of f_1 and f_3 are compared for tie-rod 1 and tie-rod 2, one may observe that conditions T4, T5 and T6 may be associated to a different structural condition with respect to condition T0 (see Table 3). Anyway, this remark comes from a comparison between the monitored structure, i.e. tie-rod 1, and a reference structure, i.e. tie-rod 2. In this way, an anomaly can be detected only by a comparison between the behaviour of two similar structures, assuming that one is not damaged, under the same environmental and operational variations, which it is not always possible in real applications. In addition, it is important to notice that no distinction may be made between conditions T4, T5 and T6 and that the application of masses close to the constraints cannot be clearly detected.

About the MAC, the four mode shapes identified at the beginning of the monitoring period on each of the two tie-rods have been set as a reference. The trends of the MAC confirmed what already seen in the simulation phase: even if the coefficients obtained from real data are slightly lower than those observed in Figure 11, they are close to 1, with a significant variability mainly caused by the modal identification uncertainty. Furthermore, as the mode order increases, the related MAC coefficient is more sensitive to the presence of simulated damage. When the damage is simulated at midspan, MAC coefficients associated to odd modes change more than those related to even modes. Nevertheless, no clear statements on the health state of the tie-rod can be directly made, due to the above-mentioned coefficient dispersion. The trends in time of the MAC coefficients are not presented, to avoid redundant figures, while attention has been mainly focused on the trends of the eigenfrequencies, which allowed for an easier visualization of the results.

In the following, it is showed that the proposed damage detection strategy overcomes all the above-mentioned limitations allowing one to evaluate each condition T1-T6 against T0, without the need to considering all the data in the monitoring period and without a comparison with a reference structure.

The results obtained by evaluating the two damage indexes DI_1 and DI_2 from the identified modal parameters are reported in Figure 16 and Figure 17 for tie-rod 1. In order to apply the strategy, the baseline is the period between 19th December and 28th December, indicated with black crosses. The set of modal parameters related to this period has been used to define the threshold t_{exc}, indicated with a black dashed line in the following plots.

The period between 29th December and 4th January is indicated with blue circles; in this case, tie-rod 1 is still under reference conditions, i.e. blue circles should fall under the threshold. Then the points when tie-rod 1 was subject to simulated damage are represented with red triangles. Different periods of the experimental tests corresponding to different masses in different positions are separated by vertical lines and labelled according to Table 3. To allow for a clear representation, shrinking data, the time resolution of the following plots has been reduced by applying a moving average of two hours.

Before discussing the results, it is worth pointing out that the automatic modal identification was particularly difficult during some periods of the experimental tests. Considering that the adopted algorithm for the modal identification relies on the hypothesis of an input which is white noise, in many different occasions this assumption does not hold in the specific environment where the test-case is located. The ongoing activities in the surroundings of the experimental set-up occasionally caused a difficult identification which reflects in more scattered damage indexes (see conditions T1, T2 in Figure 16 and Figure 17). These identification problems have a higher impact on the estimate of the MAC rather than on the eigenfrequencies. Indeed, small variations in the modal coordinates are responsible for high variations in the MAC, further magnified by the MSD.

The index DI_1 for tie-rod 1 is shown in Figure 16. It is possible to see that only a single false alarm is reported, since only one blue point is above the threshold. Furthermore, all the simulated damages T1-T6 are properly detected.

Considering that conditions T1, T2 and T3 refer to the addition of concentrated masses close to one of the clamps ($\xi = \mathrm{L}/10$), while conditions T4, T5 and T6 refer to the addition of the masses at midspan ($\xi = \mathrm{L}/2$), in both cases the index increases when the added mass increases.

Considering pairs of conditions with same mass but different positions (T3 and T4, T2 and T5, T1 and T6), it is possible to recognize that the index is more sensitive when damage is simulated at midspan rather than when it is close to the constraints.

It is also possible to observe that conditions T2, T3, T4 and T5 are always detected with no false negative reported; conversely when the smallest mass of 1% is applied to the structure (conditions T1 and T6), a number of false negatives is observed, with red triangles that fall under the threshold. This happens more often for condition T1, where the marker dispersion is higher, due to the above-mentioned problems related to the automatic modal identification. Nevertheless, conditions T1 and T6 can be visually and generally distinguished from condition T0.

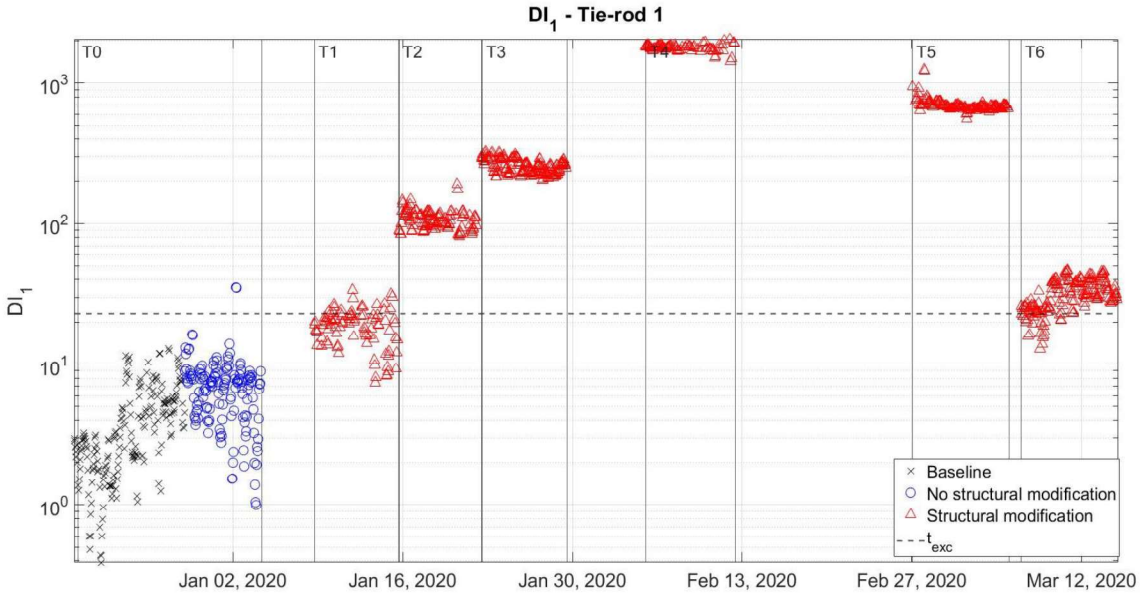

Figure 16: Damage index DI_1 for real data referring to tie-rod 1. Black crosses indicate the observations used as baseline, blue circles are used to indicate undamaged data, red triangles refer to the damage condition; the threshold t_{exc} is indicated by a black dashed line

The results referring to DI_2 for tie-rod 1 are reported in Figure 17. Some blue circles are above the threshold indicating some false alarms. In this case, considering the period when different masses were added to the tie-rod, the index is always able to clearly detect the simulated damage, even when the entity of the mass is 1 %, both at midspan (T6) and close to the boundaries (T1). Comparing these results with those in Figure 16, the index DI_2 is more sensitive than DI_1, confirming what already noted for simulated data. By looking at conditions T4, T5 and T6, it is observed that the damage index increases as the mass increases. Anyway, the points are more scattered than what obtained with DI_1, thus no clear indication about the relative entity of the structural modification can be stated if T1, T2 and T3 are considered. When the quality of the modal identification improves, DI_2 provides more stable results, even when the smallest damage condition is simulated (see condition T6 in Figure 17).

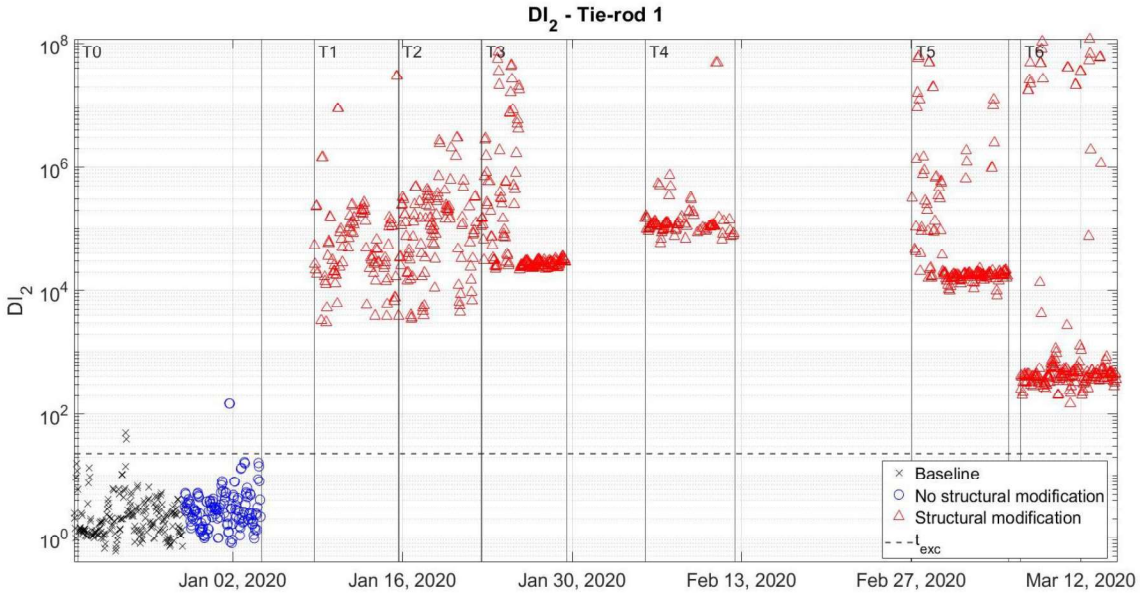

Figure 17: Damage index DI_2 for real data referring to tie-rod 1. Black crosses indicate the observations used as baseline, blue circles are used to indicate undamaged data, red triangles refer to the damage condition; the threshold t_{exc} is indicated by a black dashed line

In order to summarize the information provided by the indexes DI_1 and DI_2, accounting for the different dispersion that may be observed depending on the quality of the modal identification, a stabilization criterion may be introduced. Indeed, if all the samples of a damage index observed in a single day are collected in a vector $\underline{DI}$ ($\underline{DI}$ may contain either values of DI_1 or DI_2 and the procedure is the same for both), the overall daily behaviour may be resumed by $\mu_{\underline{DI}} \pm 2\sigma_{\underline{DI}}$, where $\mu_{\underline{DI}}$ and $\sigma_{\underline{DI}}$ are the mean and standard deviation of all the elements of $\underline{DI}$. By comparing this value against the threshold t_{exc} a decision on the health state of the tie-rod may be taken, as shown in Figure 18, where a different alert level (AL) may be reached according to the following conditions:

1. If $\left(\mu_{\underline{DI}} + 2\sigma_{\underline{DI}}\right) < t_{\text{exc}}$ the tie-rod is in the reference condition (AL "Healthy" in Figure 18).
2. If $\left(\mu_{\underline{DI}} - 2\sigma_{\underline{DI}}\right) > t_{\text{exc}}$ the tie-rod is damaged (AL "Damage" in Figure 18).
3. If $\left(\mu_{\underline{DI}} - 2\sigma_{\underline{DI}}\right) < t_{\text{exc}} < \left(\mu_{\underline{DI}} + 2\sigma_{\underline{DI}}\right)$ a warning may be produced following a conservative approach (AL "Warning" in Figure 18).

Such a strategy can allow for a more robust decision on the health of the monitored tie-rod, especially when the damage index continuously passes from being below or above the threshold, because of modal identification errors.

Figure 18 shows the application of this strategy to the days referring to condition T0 (seven days, from December 29th 2019 to January 4th 2020, marked as blue circles in Figure 16 and Figure 17) and condition T6 (eight days, from March 7th 2020 to march 14th 2020). These two conditions are the furthest in time considering the sets of data collected during the experimental tests. It is also worth remembering that condition T6 refers to the smallest simulated damage (i.e. added mass of 1%).

Figure 18a and Figure 18c refer to DI_1 and DI_2 evaluated for tie-rod 1 and represent in a synthetic way what has been qualitatively observed in Figure 16 and Figure 17 respectively. Indeed, in both cases the AL is "Healthy" for all the days of condition T0, when no damage is simulated on tie-rod 1. Considering condition T6, only DI_2 always detects the damage from day 8 to day 15 (i.e. all points from day 8 to day 15 in Figure 18c reach AL "Damage"). If the decision is made on DI_1 (see Figure 18a), only the last three days, from day

13 to day 15, reach the level “Damage” whereas days from 8 to 12 are classified as “Warning”. This is in agreement with what previously observed for period T6 in Figure 16, where the index DI_1 was close to the threshold t_{exc}. The quality of the identification allows for a reduced dispersion towards the last days of the period, where damage is correctly detected. Either way, an alarm can be always produced when the structure is damaged since at least the level “Warning” is reached, thus avoiding false negatives.

In the end, Figure 18b and Figure 18d refer to DI_1 and DI_2, respectively, evaluated for tie-rod 2, where no damage has been simulated throughout all the tests. For all the 15 days the AL is at level “Healthy”, confirming that tie-rod 2 in the second week of March 2020 is still in the same condition as in the baseline set (December 19th 2019 to December 28th 2019).

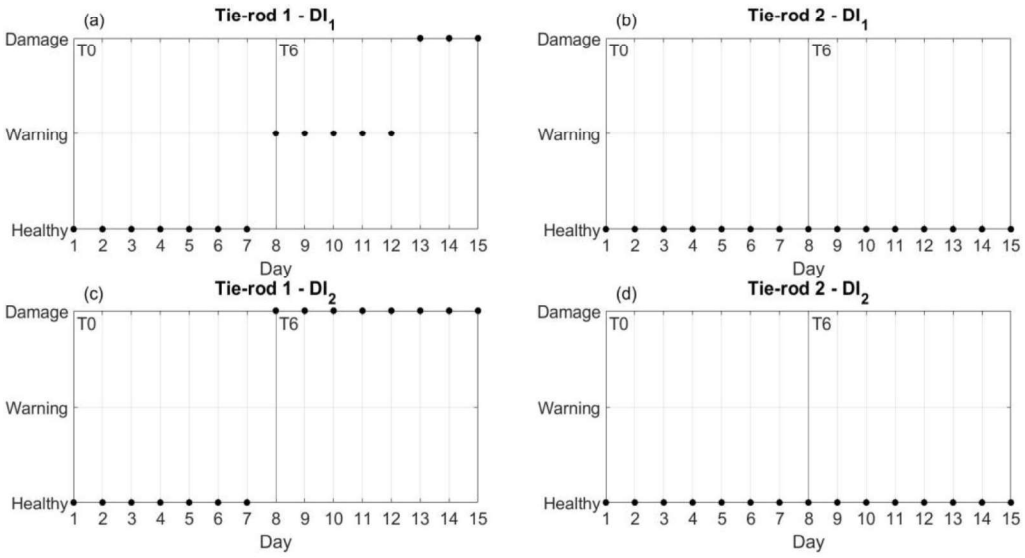

Figure 18: ALs for tie-rod 1 (a) and (c) and tie-rod 2 (b) and (d). The days 1-7 are related to condition T0, days 8-15 are related to condition T6.

To recall the main aspects emerged from the experimental tests, the index DI_2 has been proved to be more sensitive to the presence of structural variations than DI_1, as already observed in the simulations. This may suggest that the index DI_2 may be adopted to detect damage in tie-rods at an earlier stage than DI_1. On the other hand, the index DI_1 is more robust to false positives, which is a problem strictly related to the performances of the automatic identification of the modal parameters.

Thus, a pre-selection strategy may be developed to automatically discard data that could cause a less stable automatic identification of the modal parameters. In this work, only data where the automatic identification completely failed (i.e. when even one of the four vibration modes was not identified by the PLSCFD algorithm) were excluded from the analysis, while no pre-selection of the data has been carried out. This has been chosen to intentionally point out the critical aspects that may arise in a continuous automatic damage detection perspective. To solve the mentioned problem, a stabilization criterion has been proposed to automatically evaluate the health state of the monitored tie-rod; in this case any decision is based on the overall behaviour observed on a daily basis, accounting for the uncertainty related to the automatic modal identification procedure [46–50].

6. Conclusions

This paper has presented a vibration-based damage detection strategy for axially loaded beam-type structures working under realistic environment. Two damage indexes have been proposed and the validation has been performed on the case study of structural health monitoring of tie-rods. Simulations and experimental data showed that both the proposed damage indexes can detect damage in a realistic environment, without any prior knowledge of the axial load, representing an improvement with respect to the state of the art of damage detection in tie-rods.

More specifically, DI_2 (based on mode shapes) proved to be more sensitive to damage than DI_1 (based on eigenfrequencies), although this comes at the price of a lower reliability when the quality of the modal identification is poor. In such cases, more robust results can be obtained if a stabilization criterion is adopted similar to the one presented here. This point is important in a continuous structural health monitoring perspective, since a reliable automatic damage detection can be carried out also in presence of disturbances coming from the operational environment.

An interesting point is that DI_1 can be evaluated even with a single accelerometer placed in a position that is not a vibration node for the considered modes. This aspect can be important in situations where the use of few sensors is desirable for either practical or economic reasons.

A future development will be related to the testing of the indexes in a more realistic damage scenario, such as chemical corrosion, implying an actual stiffness change due to the reduction in the cross section. This aspect, together with a study on the relationship between the uncertainty of the modal identification and the dispersion of the damage indexes, will allow for a reliable estimation of the minimum detectable damage in real applications.

APPENDIX A

Given a vector $\underline{B}_1$ of size $(N_{\mathrm{rec}} \times 1)$:

$$\underline{B}_1 = \begin{Bmatrix} b_{1,1} \\ b_{2,1} \\ \vdots \\ b_{i,1} \\ \vdots \\ b_{N_{\mathrm{rec}},1} \end{Bmatrix} \tag{10}$$

$\underline{B}_1$ can be the first column of either matrix $[f]_{(N_{\mathrm{rec}} \times M)}$ or $[MAC]_{(N_{\mathrm{rec}} \times M)}$. The mean $\underline{\tilde{B}}_1$ is defined as:

$$\underline{\tilde{B}}_1 = \frac{\sum_{r=1}^{N_{\mathrm{rec}}} b_{r,1}}{N_{\mathrm{rec}}} \tag{11}$$

For two vectors $\underline{B}_1$ and $\underline{B}_2$, both of size $(N_{\mathrm{rec}} \times 1)$, the covariance is defined as [51]:

$$cov(\underline{B}_1, \underline{B}_2) = \frac{1}{N_{\mathrm{rec}} - 1} \sum_{r=1}^{N_{\mathrm{rec}}} \left(b_{r,1} - \underline{\tilde{B}}_1\right)\left(b_{r,2} - \underline{\tilde{B}}_2\right) \tag{12}$$

Considering a generic matrix $[B]_{(N_{\mathrm{rec}} \times M)}$ with N_{rec} rows and M columns ($[B]$ can be either matrix $[f]$ or matrix $[MAC]$), every j-th column, with $j = 1, \dots, M$, can be expressed as a vector $\underline{B}_j$ of size $(N_{\mathrm{rec}} \times 1)$, thus:

$$[B]_{(N_{\text{rec}}\times M)} = \{\underline{B}_1 \quad \underline{B}_2 \quad \cdots \quad \underline{B}_j \quad \cdots \quad \underline{B}_M\} \tag{13}$$

The multivariate mean vector $\underline{\mu_B}_{(M\times 1)}$ is defined as:

$$\underline{\mu_B}_{(M\times 1)} = \{\tilde{\underline{B}}_1 \quad \tilde{\underline{B}}_2 \quad \cdots \quad \tilde{\underline{B}}_j \quad \cdots \quad \tilde{\underline{B}}_M\}^T \tag{14}$$

and the covariance matrix $[\Sigma_B]_{(M\times M)}$ is defined as [51]:

$$[\Sigma_B]_{(M\times M)} = \begin{Bmatrix} cov(\underline{B}_1,\underline{B}_1) & cov(\underline{B}_1,\underline{B}_2) & \cdots & cov(\underline{B}_1,\underline{B}_M) \\ cov(\underline{B}_2,\underline{B}_1) & cov(\underline{B}_2,\underline{B}_2) & \cdots & cov(\underline{B}_2,\underline{B}_M) \\ \vdots & \vdots & \ddots & \vdots \\ cov(\underline{B}_M,\underline{B}_1) & cov(\underline{B}_M,\underline{B}_2) & \cdots & cov(\underline{B}_M,\underline{B}_M) \end{Bmatrix} \tag{15}$$

The MSD [36] between a vector $\underline{z}_{(M\times 1)}$ and $[B]$ is defined as:

$$MSD(\underline{z},[B]) = \left(\underline{z}-\underline{\mu}_B\right)^T [\Sigma_B]^{-1}\left(\underline{z}-\underline{\mu}_B\right) \tag{16}$$

where the suffix "-1" means the inverse.

In order to assess whether the vector $\underline{z}$ is an outlier with respect to the multivariate set $[B]$, $MSD(\underline{z},[B])$ has to be compared against a threshold. A numeric approach based on a Monte Carlo method can be adopted to calculate such threshold, as described in [36]. The procedure is briefly described in the following steps:

1. Construct a matrix of dimension $(N_{\text{rec}} \times M)$ where every element is a random number generated from a zero mean and unit standard deviation normal distribution.
2. Calculate the MSD between each row of the matrix and the matrix itself and store the maximum value obtained, i.e. the largest of the N_{rec} MSD is stored.
3. Repeat the process for a large number of trials and then sort all the largest MSDs in terms of magnitude. The critical values for 1% or 5% tests of discordancy are then given by the MSDs in the array above which 1% or 5% of the trials occurs, obtaining what is generally indicated as the inclusive threshold t_{inc}. Thus, if $MSD(\underline{z},[B]) > t_{\text{inc}}$, $\underline{z}$ is an outlier. The term inclusive comes from the assumption that the baseline set $[B]$ also contains outliers.
4. If the baseline set does not contain outliers, the exclusive threshold t_{exc} must be adopted. More specifically, the inclusive threshold and the exclusive threshold are related by the formula [52]:

$$t_{\text{exc}} = \frac{(N_{\text{rec}}-1)(N_{\text{rec}}+1)^2 t_{\text{inc}}}{N_{\text{rec}}({N_{\text{rec}}}^2-(N_{\text{rec}}+1)t_{\text{inc}})} \tag{17}$$

   If $MSD(\underline{z},[B]) > t_{\text{exc}}$, $\underline{z}$ is an outlier.

In this work, the exclusive threshold t_{exc} has been calculated following the above-mentioned procedure, considering $N_{\text{rec}} = N_{\text{rec}}^{\text{base}}$, where $N_{\text{rec}}^{\text{base}}$ is the number of records of vibration data acquired when the structure is in a healthy condition, M equal to the number of considered vibration modes, a number of 1000 iterations and critical value for 1% test of discordancy.

Bibliography

[1] C.R. Farrar, K. Worden, An introduction to structural health monitoring, CISM Int. Cent. Mech. Sci. Courses Lect. 520 (2010) 1–17. https://doi.org/10.1007/978-3-7091-0399-9_1.

[2] C.R. (Charles R.. Farrar, K. Worden, Structural health monitoring: a machine learning perspective, (2012).

[3] S.W. Doebling, C.R. Farrar, M.B. Prime, A summary review of vibration-based damage identification methods, Shock Vib. Dig. 30 (1998) 91–105. https://doi.org/10.1177/058310249803000201.

[4] W. Fan, P. Qiao, Vibration-based damage identification methods: A review and comparative study, Struct. Heal. Monit. 10 (2011) 83–111. https://doi.org/10.1177/1475921710365419.

[5] H. Sohn, Effects of environmental and operational variability on structural health monitoring, Philos. Trans. R. Soc. A Math. Phys. Eng. Sci. 365 (2007) 539–560. https://doi.org/10.1098/rsta.2006.1935.

[6] R. Hou, Y. Xia, Review on the new development of vibration-based damage identification for civil engineering structures: 2010–2019, J. Sound Vib. 491 (2021) 115741. https://doi.org/10.1016/j.jsv.2020.115741.

[7] E. Coïsson, L. Collini, L. Ferrari, R. Garziera, K. Riabova, Dynamical Assessment of the Work Conditions of Reinforcement Tie-Rods in Historical Masonry Structures, Int. J. Archit. Herit. 13 (2019) 358–370. https://doi.org/10.1080/15583058.2018.1563231.

[8] S.B. Briccoli, T. Ugo, Experimental Methods for Estimating In Situ Tensile Force in Tie-Rods, J. Eng. Mech. 127 (2001) 1275–1283.

[9] N. Tullini, G. Rebecchi, F. Laudiero, Bending tests to estimate the axial force in tie-rods, Mech. Res. Commun. 44 (2012) 57–64. https://doi.org/10.1016/j.mechrescom.2012.06.005.

[10] C. Blasi, S. Sorace, Determining the Axial Force in Metallic Rods, Struct. Eng. Int. 4 (1994) 241–246. https://doi.org/10.2749/101686694780601809.

[11] A. De Falco, C. Resta, G. Sevieri, Sensitivity analysis of frequency-based tie-rod axial load evaluation methods, Eng. Struct. 229 (2021) 111568. https://doi.org/10.1016/j.engstruct.2020.111568.

[12] C. Resta, G. Chellini, A. De Falco, Dynamic assessment of axial load in tie-rods by means of acoustic measurements, Buildings. 10 (2020). https://doi.org/10.3390/buildings10020023.

[13] G. Rebecchi, N. Tullini, F. Laudiero, Estimate of the axial force in slender beams with unknown boundary conditions using one flexural mode shape, J. Sound Vib. 332 (2013) 4122–4135. https://doi.org/10.1016/j.jsv.2013.03.018.

[14] N. Tullini, F. Laudiero, Dynamic identification of beam axial loads using one flexural mode shape, J. Sound Vib. 318 (2008) 131–147. https://doi.org/10.1016/j.jsv.2008.03.061.

[15] S. Lagomarsino, C. Calderini, The dynamical identification of the tensile force in ancient tie-rods, Eng. Struct. 27 (2005) 846–856. https://doi.org/10.1016/j.engstruct.2005.01.008.

[16] L. Collini, R. Garziera, K. Riabova, Vibration Analysis for Monitoring of Ancient Tie-Rods, Shock Vib. 2017 (2017). https://doi.org/10.1155/2017/7591749.

[17] T. Kernicky, M. Whelan, E. Al-Shaer, Dynamic identification of axial force and boundary restraints in tie rods and cables with uncertainty quantification using Set Inversion Via Interval Analysis, J. Sound Vib. 423 (2018) 401–420. https://doi.org/10.1016/j.jsv.2018.02.062.

[18] S. Campagnari, F. Di Matteo, S. Manzoni, M. Scaccabarozzi, M. Vanali, Estimation of axial load in tie-rods using experimental and operational modal analysis, J. Vib. Acoust. Trans. ASME. 139 (2017). https://doi.org/10.1115/1.4036108.

[19] C. Gentilini, A. Marzani, M. Mazzotti, Nondestructive characterization of tie-rods by means of dynamic testing, added masses and genetic algorithms, J. Sound Vib. 332 (2013) 76–101. https://doi.org/10.1016/j.jsv.2012.08.009.

[20] L. Collini, R. Garziera, K. Riabova, Detection of cracks in axially loaded tie-rods by vibration analysis, Nondestruct. Test. Eval. 35 (2020) 121–138. https://doi.org/10.1080/10589759.2019.1649400.

[21] K. Maes, J. Peeters, E. Reynders, G. Lombaert, G. De Roeck, Identification of axial forces in beam members by local vibration measurements, J. Sound Vib. 332 (2013) 5417–5432. https://doi.org/10.1016/j.jsv.2013.05.017.

[22] C. Rainieri, D. Gargaro, L. Cieri, G. Fabbrocino, Vibration-based continuous monitoring of tensile loads in cables and rods: System development and application, Struct. Heal. Monit. 5 (2014) 271–278. https://doi.org/10.1007/978-3-319-04570-2__30.

[23] C. Rainieri, G. Fabbrocino, Development and validation of an automated operational modal analysis algorithm for vibration-based monitoring and tensile load estimation, Mech. Syst. Signal Process. 60 (2015) 512–534. https://doi.org/10.1016/j.ymssp.2015.01.019.

[24] F. Cheli, G. Diana, Advanced dynamics of mechanical systems, 2015. https://doi.org/10.1007/978-3-319-18200-1.

[25] B.L. Clarkson, Theory of vibration with applications, J. Sound Vib. 79 (1981) 627. https://doi.org/10.1016/0022-460x(81)90474-0.

[26] C.M. Harris, A.G. Piersol, Shock and Vibration Handbook, 1962. https://doi.org/10.1063/1.3058392.

[27] E. Cescatti, F. Da Porto, C. Modena, Axial Force Estimation in Historical Metal Tie-Rods: Methods, Influencing Parameters, and Laboratory Tests, Int. J. Archit. Herit. 13 (2019) 317–328. https://doi.org/10.1080/15583058.2018.1563234.

[28] D.J. Ewins, Modal Testing: Theory, Practice and Application, (2001) 562. http://www.amazon.com/Modal-Testing-Application-Mechanical-Engineering/dp/0863802184.

[29] C. Rainieri, G. Fabbrocino, E. Cosenza, Near real-time tracking of dynamic properties for standalone structural health monitoring systems, Mech. Syst. Signal Process. 25 (2011) 3010–3026. https://doi.org/10.1016/j.ymssp.2011.04.010.

[30] E. Reynders, J. Houbrechts, G. De Roeck, Fully automated (operational) modal analysis, Mech. Syst. Signal Process. 29 (2012) 228–250. https://doi.org/10.1016/j.ymssp.2012.01.007.

[31] E. Neu, F. Janser, A.A. Khatibi, A.C. Orifici, Fully Automated Operational Modal Analysis using multi-stage clustering, Mech. Syst. Signal Process. 84 (2017) 308–323. https://doi.org/10.1016/j.ymssp.2016.07.031.

[32] P. Charbonnel, Fuzzy-driven strategy for fully automated modal analysis: Application to the SMART2013 shaking-table test campaign, Mech. Syst. Signal Process. 152 (2021) 107388. https://doi.org/10.1016/j.ymssp.2020.107388.

[33] M. He, P. Liang, J. Li, Y. Zhang, Y. Liu, Fully automated precise operational modal identification, Eng. Struct. 234 (2021) 111988. https://doi.org/10.1016/j.engstruct.2021.111988.

[34] B. Peeters, H. Van Der Auweraer, P. Guillaume, J. Leuridan, The PolyMAX frequency-domain method : a new standard for modal parameter estimation?, Shock Vib. 11 (2004) 395–409. https://doi.org/10.1155/2004/523692.

[35] C. Rainieri, G. Fabbrocino, Operational Modal Analysis of Civil Engineering Structures, Oper. Modal Anal. Civ. Eng. Struct. (2014). https://doi.org/10.1007/978-1-4939-0767-0.

[36] K. Worden, G. Manson, N.R.J. Fieller, Damage detection using outlier analysis, J. Sound Vib. 229

(2000) 647–667. https://doi.org/10.1006/jsvi.1999.2514.

[37] E. Figueiredo, G. Park, C.R. Farrar, K. Worden, J. Figueiras, Machine learning algorithms for damage detection under operational and environmental variability, Struct. Heal. Monit. (n.d.).

[38] A. Deraemaeker, K. Worden, A comparison of linear approaches to filter out environmental effects in structural health monitoring, Mech. Syst. Signal Process. 105 (2018) 1–15. https://doi.org/10.1016/j.ymssp.2017.11.045.

[39] R. Brincker, L. Zhang, P. Andersen, Modal identification of output-only systems using frequency domain decomposition, Smart Mater. Struct. 10 (2001) 441–445. https://doi.org/10.1088/0964-1726/10/3/303.

[40] A. Brandt, Noise and vibration analysis - Signal analysis and experimental procedures, Wiley, 2011.

[41] S. Banerjee, F. Ricci, E. Monaco, A. Mal, A wave propagation and vibration-based approach for damage identification in structural components, J. Sound Vib. 322 (2009) 167–183. https://doi.org/10.1016/j.jsv.2008.11.010.

[42] A. Sarrafi, Z. Mao, C. Niezrecki, P. Poozesh, Vibration-based damage detection in wind turbine blades using Phase-based Motion Estimation and motion magnification, J. Sound Vib. 421 (2018) 300–318. https://doi.org/10.1016/j.jsv.2018.01.050.

[43] A. Theodosiou, M. Komodromos, K. Kalli, Carbon Cantilever Beam Health Inspection Using a Polymer Fiber Bragg Grating Array, J. Light. Technol. 36 (2018) 986–992. https://doi.org/10.1109/JLT.2017.2768414.

[44] C.S. Sakaris, J.S. Sakellariou, S.D. Fassois, Random-vibration-based damage detection and precise localization on a lab–scale aircraft stabilizer structure via the Generalized Functional Model Based Method, Struct. Heal. Monit. 16 (2017) 594–610. https://doi.org/10.1177/1475921717707903.

[45] W.J. Yi, Y. Zhou, S. Kunnath, B. Xu, Identification of localized frame parameters using higher natural modes, Eng. Struct. 30 (2008) 3082–3094. https://doi.org/10.1016/j.engstruct.2008.04.012.

[46] R. Pintelon, P. Guillaume, J. Schoukens, Uncertainty calculation in (operational) modal analysis, Mech. Syst. Signal Process. 21 (2007) 2359–2373. https://doi.org/10.1016/j.ymssp.2006.11.007.

[47] E. Reynders, R. Pintelon, G. De Roeck, Uncertainty bounds on modal parameters obtained from stochastic subspace identification, Mech. Syst. Signal Process. 22 (2008) 948–969. https://doi.org/10.1016/j.ymssp.2007.10.009.

[48] M. Döhler, X.B. Lam, L. Mevel, Uncertainty quantification for modal parameters from stochastic subspace identification on multi-setup measurements, Mech. Syst. Signal Process. 36 (2013) 562–581. https://doi.org/10.1016/j.ymssp.2012.11.011.

[49] M. Modares, R.L. Mullen, Dynamic Analysis of Structures with Interval Uncertainty, J. Eng. Mech. 140 (2014) 04013011. https://doi.org/10.1061/(asce)em.1943-7889.0000660.

[50] S. Greś, M. Döhler, L. Mevel, Uncertainty quantification of the Modal Assurance Criterion in operational modal analysis, Mech. Syst. Signal Process. 152 (2021). https://doi.org/10.1016/j.ymssp.2020.107457.

[51] K. Il Park, Fundamentals of probability and stochastic processes with applications to communications, 2017. https://doi.org/10.1007/978-3-319-68075-0.

[52] C.R. Farrar, K. Worden, Structural health monitoring: a machine learning perspective, (2013).